Sulfur Oxidation States Manipulate Excited State Electronic Configurations for Constructing Highly Efficient Organic Type I Photosensitizer

Jianye Gong,[a] Xiaopeng Wang,[a] Weijing Zhang,[b] Yifan Wu,[a] Kai Li,[a] Renmanduhu Sha,[a] Lingxiu Liu,[a] Chunbin Li,[a] Lina Feng,[a] Guoyu Jiang,[a] Jianguo Wang*[a] and Ben Zhong Tang[c]

[a] J. Gong, X. Wang, Y. Wu, K. Li, R. Sha, L. Liu, C. Li, L. Feng, Prof. G. Jiang, Prof. J. Wang
College of Chemistry and Chemical Engineering
Inner Mongolia Key Laboratory of Fine Organic Synthesis Department
Inner Mongolia University
Hohhot 010021, P. R. China
E-mail: wangjg@iccas.ac.cn

[b] W. Zhang
Xi'an Modern Chemistry Research Institute
Xi'an 710069, P. R. China

[c] B. Z. Tang
School of Science and Engineering, Shenzhen Institute of Aggregate Science and Technology,
The Chinese University of Hong Kong, Shenzhen (CUHK-Shenzhen)
Shenzhen, Guangdong 518172, P. R. China

Experimental procedures

Materials

N,N-diphenyl-4-(4,4,5,5-tetramethyl-1,3,2-dioxaborolan-2-yl)aniline and 4-methoxy-N-(4-methoxyphenyl)-N-(4-(4,4,5,5-tetramethyl-1,3,2-dioxaborolan-2-yl)phenyl)aniline were purchased from Soochiral chemistry. 2,8-dibromodibenzo[*b*,*d*]thiophene was purchased from Leyan. All other chemicals and reagents were purchased from Admas-beta® and used directly without further purification. Phosphate buffered solution (PBS, 10 mM, pH 7.4), 2',7'-dichlorodihydrofluorescein diacetate (DCFH-DA), aminophenyl fluorescein (APF), hydroxyphenyl fluorescein (HPF), dihydrorhodamine 123 (DHR123), 9,10-anthracenediyl-bis(methylene) dimalonic acid (ABDA), 5-tert-butoxycarbonyl-5-methyl-1-pyrroline-N-oxide (BMPO), 4-amino-2,2,6,6-tetramethylpiperidine (TEMP), calcein acetoxymethyl ester (Calcein-AM), propidium iodide (PI) were purchased from Sigma-Aldrich. Thiazolyl blue tetrazolium bromide (MTT) was purchased from Beyotime biotechnology Co., Ltd. The *S. aureus* (BNCC 186335) and MRSA (BNCC 337371) were purchased from BeNa Culture Collection. The *E.coli* was obtained from the Engineering Research Center of Dairy Quality and Safety Control Technology Ministry of Education of Inner Mongolia University.

Instruments

^{1}H and ^{13}C NMR spectra were recorded with Bruker ARX 500/600 NMR spectrometer using tetramethylsilane (TMS) as a reference. High resolution mass spectra (HRMS) were measured with a LCMS9030 spectrometer. UV-vis absorption spectra were recorded on a SHIMADZU UV-2600i spectrophotometer. Photoluminescence (PL) spectra were recorded on a HITACHI F-4700 fluorescence spectrophotometer. Single crystal X-ray diffraction was performed on a Rigaku Oxford Diffraction Supernova Dual Source, Cu at Zero equipped with an AtlasS2 CCD using Cu Kα radiation. The data were collected and processed using CrysAlisPro. Size distribution and zeta potential were analyzed on a dynamic light scattering (DLS) using an Omni NanoBrook. The absorbance of each sample was measured using a microplate reader (BioTek) for MTT assay. The bacterial fluorescence images were taken by inverted fluorescence microscope (Nikon Ti2) or confocal laser scanning microscope (LSM880, ZEISS, Germany). The bacterial morphology was observed on a HITACHI S-4800 scanning electron microscope. The photographs of agar plate were taken by an automated colony counter (Shineso Icount33).

Density functional theory calculations

The frontier molecular orbitals were calculated at the level of M06-2X/6-311G(d) by Gaussian 09 program.[1] The Hirshfeld surfaces and decomposed fingerprint plots were mapped using Crystal Explorer 17.5 package.[2] The independent gradient model (IGM) analysis[3] of weak interaction based on single crystal structure was conducted by using Multiwfn program[4] The corresponding structure and IGM isosurfaces were generated using visual molecular dynamics (VMD) program.[5] The electrostatic potential (ESP) characteristic parameters were calculated based on the single crystal structure with electronic wave function information using Multiwfn. The visualization of the ESP distribution was performed using GaussView 6.0. Geometries of DBTS, DBTSO, and DBTS2O at ground state were optimized at the level of M06-2X/6-311G(d)

by Gaussian 09 program. On the basis of the optimized geometries, time-dependent density functional theory (TD-DFT) was utilized at the same level to calculate the first singlet state (S_1) and the first triplet state (T_1). The natural transition orbitals (NTOs) analysis was further carried out by Multiwfn to obtain the main NTOs contributing to the electron transition. The atomic contribution and phase analysis were further performed.

Total ROS detection by DCFH

A commonly used ROS indicator 2', 7'-dichlorodihydrofluorescein diacetate (DCFH-DA) was utilized to detect the total ROS generation of DBTS, DBTSO and DBTS2O in PBS under white light irradiation (100 mW cm^{-2}), as well as 2OA and Ce6 in PBS under white light irradiation (8 mW cm^{-2}). Briefly, 0.5 mL DCFH-DA in ethanol (1×10^{-3} M) was added to 2 mL NaOH (1×10^{-2} M) and allowed to be stirred at room temperature for 30 min. Then the hydrolysate was neutralized with 10 mL of PBS at pH 7.4, and kept in dark before use. By the time, DCFH-DA was hydrolyzed to DCFH. Then the ROS indicator (4×10^{-5} M) in PBS was further diluted to 1×10^{-6} M in the sample solution of DBTS, DBTSO, DBTS2O, 2OA or Ce6 (5×10^{-6} M) for measurement by PL instrument. The fluorescence of 2', 7'-dichlorofluorescein triggered by PS sensitized ROS under white light irradiation was recorded at different time intervals. The PL spectra were measured with excitation at 489 nm and emission was collected from 500 to 600 nm. The fluorescence intensity at 523 nm was recorded to indicate the total ROS generation rate of DBTS, DBTSO or DBTS2O. The fluorescence intensity at 530 nm was recorded to indicate the total ROS generation rate of 2OA and Ce6.

Detection of •OH generation by APF

The •OH generation measurements were performed using aminophenyl fluorescein (APF) as an indicator. The stock solution of APF (5 mM) was diluted to 5 μM in the sample solution of DBTS, DBTSO or DBTS2O (5×10^{-6} M) in PBS. The fluorescence signal of APF was monitored at different time intervals in a range of 500-600 nm with the excitation wavelength at 490 nm after the solution was irradiated by white light irradiation (100 mW cm^{-2}). The fluorescence intensity at 515 nm was recorded to indicate the •OH generation rate of DBTS, DBTSO or DBTS2O.

Detection of •OH generation by HPF

The •OH generation measurements were performed using hydroxyphenyl fluorescein (HPF) as an indicator. The stock solution of HPF (5 mM) was diluted to 5 μM in the sample solution of 2OA or Ce6 (5×10^{-6} M) in PBS. The fluorescence signal of HPF was monitored at different time intervals in a range of 500-600 nm with the excitation wavelength at 490 nm after the solution was irradiated by white light irradiation (8 mW cm^{-2}). The fluorescence intensity at 521 nm was recorded to indicate the •OH generation rate of 2OA and Ce6.

Detection of $O_2^{\bullet-}$ generation by DHR123

The $O_2^{\bullet-}$ generation measurements were performed using dihydrorhodamine 123 (DHR123) as an indicator. The stock solution of DHR 123 (1 mM) was diluted to 5 μM in the sample solution of DBTS, DBTSO, DBTS2O, 2OA or Ce6 (5×10^{-6} M) in PBS. The fluorescence signal of DHR 123 was monitored at different time intervals in a range of 500-600 nm with the

excitation wavelength at 480 nm after the solution was irradiated by white light irradiation (DBTS/DBTSO/DBTS2O: 100 mW cm^{-2}, 2OA/Ce6: 8 mW cm^{-2}). The fluorescence intensity at 527 nm was recorded to indicate the $O_2^{\bullet-}$ generation rate of DBTS, DBTSO or DBTS2O. The fluorescence intensity at 534 nm was recorded to indicate the $O_2^{\bullet-}$ generation rate of 2OA and Ce6.

Detection of $^1O_2$ generation by ABDA

For $^1O_2$ detection indicated by 9,10-anthracenediyl-bis(methylene)-dimalonic acid (ABDA), the stock solution of ABDA (5 mM) was diluted to 40 μM in the sample solution of DBTS, DBTSO or DBTS2O (5×10^{-6} M) and 50 μM in the sample solution of 2OA or Ce6 (5×10^{-6} M) in PBS. The absorption spectra of ABDA were monitored in a range of 325-425 nm after the solution was irradiated by white light irradiation (DBTS/DBTSO/DBTS2O: 100 mW cm^{-2}, 2OA/Ce6: 8 mW cm^{-2}). The absorbance decrease of ABDA at 380 nm was recorded to indicate the $^1O_2$ generation rate of DBTS, DBTSO, DBTS2O, 2OA or Ce6.

ESR analysis

ESR measurement was used to identify the type of ROS using 5-tert-butoxycarbonyl-5-methyl-1-pyrroline-N-oxide (BMPO) as the radical indicator and 2,2,6,6-tetramethylpiperidine (TEMP) as the $^1O_2$ indicator. Samples were prepared by mixing 200 μL of DBTS (20 μM), DBTSO (20 μM) or DBTS2O (20 μM) in water and 200 μL of BMPO (100 mM) or TEMP (25 mM) in water. ESR signals were recorded by adding samples through a capillary tube under a white light irradiation at 100 mW cm^{-2} for 5 min.

Bacteria culture

A single colony of *S. aureus*, MRSA or *E. coli* on LB agar was transferred to 10 mL of LB liquid culture medium and grown for 10 h at 37 °C with a shaking speed of 220 rpm. Bacteria were harvested by centrifuging at 4000 rpm for 7 min and washed twice with PBS. After removal of the supernatant, the remaining bacteria were resuspended in PBS, and diluted to an optical density of 1.0 at 600 nm (OD_{600} = 1.0 with about 10^9 CFU mL^{-1}).

Bacteria staining and imaging

After harvested by centrifugation, 1 mL of *S. aureus*, MRSA or *E. coli* solution in PBS with a density of 1×10^8 CFU mL^{-1} were mixed with 2OA (5 μM), respectively. After dispersion with vortex, the samples were incubated at 37 °C with a shaking speed of 220 rpm for 5 min, respectively. To capture fluorescence images, 2 μL of stained bacteria solution was transferred to a piece of glass slide and then covered by a coverslip. The images were collected using an inverted fluorescence microscope. Excitation wavelength: 320-430 nm, emission filter: 468-552 nm.

Antimicrobial assay

Bacteria (*S. aureus* or MRSA) at a density of ~10^8 CFU mL^{-1} were dispersed in the solutions containing 2OA (0, 1, 2, 3, 4 and 5 μM). Bacteria (*E. coli*) at a density of ~10^8 CFU mL^{-1} were dispersed in the solutions containing 2OA (0, 5 and 10 μM). These mixed solutions were then incubated at 37°C with a shaking speed of 220 rpm for 5 min. Next, the bacterial suspensions

were exposed to white light irradiation for 20 min (100 mW cm^{-2}) for phototoxicity test or were further incubated in the darkness at 37 °C for assessing the dark toxicity. Afterward, the samples were diluted to a density of ~10^2 CFU mL^{-1} with PBS and spread on the LB agar plate, followed by culturing at 37 °C for 16 h before CFU counting and taking photos.

Assessment of MIC_{90}

The MIC_{90} of 2OA was determined by incubation with *S. aureus*, MRSA or *E. coli* suspensions in LB culture medium. After incubated with different concentration of 2OA, the optical density of *S. aureus*, MRSA or *E. coli* suspensions at 600 nm was recorded at 0, 2, 4, 6, 8, 10 h.

SEM analysis

Followed by antimicrobial experiments, the bacteria were collected after irradiation and fixed with 2.5% glutaraldehyde overnight. The glutaraldehyde was removed by centrifugation and the bacteria were washed with PBS for 2 times. Then the bacteria were dehydrated with a series of graded ethanol/water solution ($v_{ethanol}$ /v_{water} =10%, 30%, 50%, 70%, 80% 90%, 100%) for 15 min each. 2 μL of bacterial suspensions were added onto clean silicon slices followed by naturally drying in the air. The specimens were coated with Au before SEM analysis.

Live/dead staining assay

Followed by antimicrobial experiments, the bacteria were collected after irradiation and incubated with Calcein-AM (10 μM) and PI (10 μM) for 1 h. Then, the bacteria were washed one time with sterile PBS. The resulting bacterial suspension (2 μL) was added onto a glass slide, which was immobilized by a clean coverslip for characterization by inverted fluorescence microscope. Excitation wavelength: 426-466 nm for Calcein-AM, 500-550 nm for PI, emission filter: 511-551 nm for Calcein-AM, 573-613 nm for PI.

Zeta potential measurements

S. aureus, MRSA or *E. coli* at a density of ~10^8 CFU mL^{-1} were incubated with 2OA (5 μM) at 37 °C with a shaking speed of 220 rpm for 5 min, respectively. The bacteria were harvested by centrifugation at 4000 rpm for 7 min and dispersed in PBS for zeta potential measurements. As for negative controls, bacterial without 2OA were treated under the same conditions.

Cell culture

LO2 cells were cultured in DMEM (containing 10% heat-inactivated FBS, 100 mg mL^{-1} penicillin and 100 mg·mL^{-1} streptomycin) at 37 °C in a humidified incubator with 5% CO_2. Before the experiments, the cells were precultured until confluence was reached.

Cell viability via MTT assay

100 μL of LO2 cell suspension (5000 cells/well) were uniformly distributed in a 96-well plate. The cells were pre-incubated for 24 h at 37 °C in a humidified incubator. Remove old media and then add 100 μL fresh medium containing various concentrations of 2OA (0 μM, 10 μM, 20 μM, 30 μM, 40 μM, 50 μM) to the plate. After co-incubating the plate for 20 h in a humidified incubator, the plate was exposed to white light irradiation (50 mW cm^{-2}) for 30 min (red) and cells without any treatment as a dark group (black). The plate was normally nurtured for

another 4 h at 37 °C. Subsequently, the serum-containing media was replaced with serum-free media and MTT reagent in cell cultures for 4 h, followed by the addition of 100 μL of DMSO to dissolve the formazan crystals. Absorbance was taken at 490 nm by a microplate reader (Biotek). The cells incubated with a culture medium was used as a control. All the experiments were performed in triplicate. The results were expressed as the viable percentage of cells after different treatments relative to the control cells without any treatment. The relative cell viability was calculated according to the following formula: Cell viability (%) = (OD_{sample} - $OD_{background}$)/($OD_{control}$ - $OD_{background}$) × 100%.

Hemolysis test

The erythrocytes were obtained by centrifuging the mouse blood (2000 rpm, 10 min). PBS was used to wash the obtained erythrocytes for three times, and then the purified erythrocytes were further diluted to a final concentration of 5% (*v*/*v*) with 0.1% Triton x-100 (1 mL) as positive group, PBS buffer (1 mL) as negative group and PBS buffer containing 5 μM or 10 μM of 2OA (1 mL) as experimental samples. Then, all the samples were shaken in an incubator at 37 °C for 1 h with a shaking speed of 100 rpm. After that, the microplate well contents were centrifuged (at 2000 rpm) for 10 min and the supernatant (100 μL) was then added into a new 96-well microplate. The absorbance of the solution was read at 540 nm by a microplate reader (Biotek). The hemolysis percentage was calculated from the following formula: Hemolysis rates = (sample absorbance-negative absorbance)/(positive absorbance-negative absorbance)×100%.

In vivo assay against MRSA

BALB/c mice (6-8 weeks old, average body weight 16-18 g) were purchased from SPF Biotechnology Co., Ltd. (Beijing, China) and all animals received care in compliance with the guidelines outlined in the Guide for the Care and Use of Laboratory Animals. All procedures were approved by the Institutional Animal Care and Use Committee at the Inner Mongolia University (IMU-2022-mouse-047). The mice were randomly divided into four groups: (1) MRSA-infected group with PBS in darkness; (2) MRSA-infected group with PBS plus white light irradiation treatment; (3) MRSA-infected group with 2OA in darkness; (4) MRSA-infected group with 2OA plus white light irradiation treatment. The mice were anesthetized by injection of 1% pentobarbital sodium saline solution (5 $mL \cdot kg^{-1}$), and hair removal cream was used to remove the hair on their backs for subsequent experiments. Next, a full-thickness skin wound with a diameter of 1 cm was made on the back of each mouse. Bacterial suspension (100 μL, 1×10^8 CFU mL^{-1}) was dripped on the surface of wounds, and the bacterial suspension were kept in the wounds for 30 min. Thirty min later, 50 μL of PBS or 2OA (5 μM) was sprayed on infected wounds for another 10 min, and treated with or without white light irradiation (100 mW cm^{-2}) for 20 min. In sterile environment, mice were fed separately in different cages to facilitate wound healing after operation. The wound sizes were imaged by a video camera and calculated at designated time intervals.

Histological Analysis

The wounds were histologically analyzed at day 9 post operation. Wound tissues were collected and fixed in 4% formaldehyde solution. The pathological sections of wound tissues were analyzed by H&E staining. Histological images were taken by an inverted microscopy.

Biosafety Assessment

To further evaluate the safety of different treatments *in vivo*, blood samples were collected from mice with various treatments at day 9 for complete blood panel analysis. White blood cell (WBC) counts, lymphocyte counts (Lymph#), neutrophil counts (Gran#), red blood cell (RBC), hemoglobin (HGB), mean corpuscular volume (MCV), mean corpuscular hemoglobin (MCH), red blood cell volume distribution width (RDW) and platelets (PLT) were measured. For biochemical blood analysis, alanine aminotransferase (ALT), transaminase (AST), albumin (ALB), blood urea nitrogen (BUN), creatinine (CREA) and uric acid (UA) were measured.

Synthesis and characterization

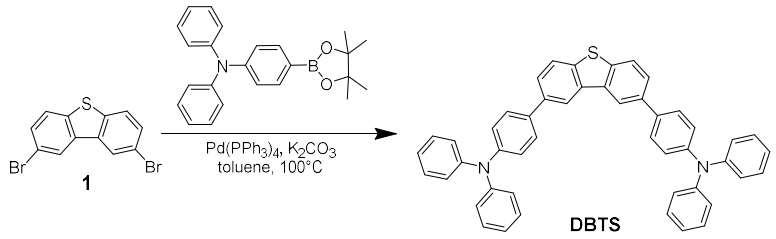

Scheme S1. Synthetic routes to DBTS.

Synthesis of **DBTS**: To a 100 mL two-neck flask equipped was added 2,8-dibromodibenzo[*b*,*d*]thiophene (181 mg, 0.53 mmol), N,N-diphenyl-4-(4,4,5,5-tetramethyl-1,3,2-dioxaborolan-2-yl)aniline (526 mg, 1.2 mmol) and $Pd(PPh_3)_4$ (62 mg, 0.053 mmol). The solids were placed under an atmosphere of N_2. Freshly distilled toluene (10 mL) and 2.0 M aq. K_3PO_4 (3 eq) was added via syringe. The reaction mixture was refluxed for 16 h at 100 °C. Then, the reaction was cooled to room temperature. The resulting slurry was suspended in CH_2Cl_2 (75 mL) and washed with H_2O (3×75 mL) followed by saturated aq. NH_4Cl (3×25 mL). The organic layer was collected, dried over Na_2SO_4, filtered, and concentrated under reduced pressure. The crude product was purified by silica gel column chromatography using petroleumether/ethyl acetate (*v*:*v*, 5:1) as an eluent to afford a white solid (213 mg, 60% yield). ^{1}H NMR (500 MHz, $CDCl_3$) δ 8.39 (s, 2H), 7.91 (d, J = 8.3 Hz, 2H), 7.71 (d, J = 8.2 Hz, 2H), 7.61 (d, J = 8.5 Hz, 4H), 7.30 (t, J = 8.1 Hz, 8H), 7.21 (d, J = 8.5 Hz, 4H), 7.18 (d, J = 7.7 Hz, 8H), 7.06 (t, J = 7.3 Hz, 4H); ^{13}C NMR (126 MHz, $CDCl_3$) δ 147.71, 147.26, 138.55, 137.48, 136.17, 135.08, 129.36, 128.06, 125.92, 124.45, 124.11, 123.13, 123.00, 119.58; HRMS: *m*/*z:* $[M+H]^+$ calcd for $[C_{48}H_{35}N_2S]^+$: 671.25209; found: 671.25155.

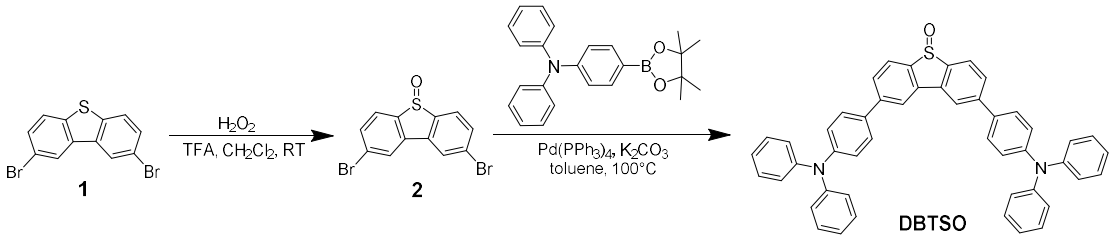

Scheme S2. Synthetic routes to DBTSO.

Synthesis of **2**: To a 100 mL round bottom flask was added 2,8-dibromodibenzo[*b*,*d*]thiophene (342 mg, 1 mmol), 30% H_2O_2 aqueous solution (148 mg, 1.3 mmol), trifluoroacetic acid (5 mL) and CH_2Cl_2 (5 mL). The resulting suspension was stirred at room temperature for 5 h and quenched by drop wise addition of saturated aq. $NaHCO_3$ (5 mL) over 20 min. The resulting slurry was suspended in CH_2Cl_2 (75 mL) and washed with H_2O (3×75 mL). The organic layer was collected, dried over Na_2SO_4, filtered, and concentrated under reduced pressure. The crude product was recrystallized from CH_2Cl_2/hexane afford a white solid (240 mg, 67% yield). ^{1}H NMR (500 MHz, $CDCl_3$), *δ* 7.96 (s, 2H), 7.88 (d, *J* = 8.2 Hz, 2H), 7.69 (d, *J* = 8.2 Hz, 2H).

Synthesis of **DBTSO**: The synthetic process was similar to DBTS except for the change of starting materials. Pure DBTSO was isolated as yellow solid with the yield of 63%. ^{1}H NMR (500 MHz, $CDCl_3$) *δ* 8.04 (d, *J* = 8.5 Hz, 2H), 8.03 (s, 2H), 7.71 (d, *J* = 8.0 Hz, 2H), 7.55 (d, *J* = 8.6 Hz, 4H), 7.31 (t, *J* = 7.8 Hz, 8H), 7.18 (t, *J* = 7.2 Hz, 12H), 7.09 (t, *J* = 7.4 Hz, 4H); ^{13}C NMR (126 MHz, $CDCl_3$) *δ* 148.39, 147.36, 145.44, 143.43, 137.83, 132.97, 129.41, 128.06, 127.93, 127.91, 124.80, 123.44, 123.32, 119.85; HRMS: *m*/*z:* $[M]^+$ calcd for $[C_{48}H_{34}N_2OS]^+$: 686.2392; found: 686.2394.

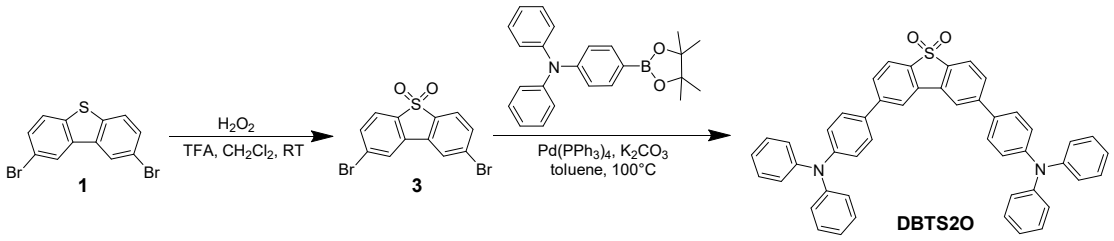

Scheme S3. Synthetic routes to DBTS2O.

Synthesis of **3**: To a 100 mL round bottom flask was added 2,8-dibromodibenzo[*b*,*d*]thiophene (342 mg, 1 mmol), 30% H_2O_2 aqueous solution (1134 mg, 10 mmol), trifluoroacetic acid (8 mL) and CH_2Cl_2 (10 mL). The resulting suspension was stirred at room temperature for 5 h and quenched by drop wise addition of saturated aq. $NaHCO_3$ (5 mL) over 20 min. The resulting slurry was suspended in CH_2Cl_2 (75 mL) and washed with H_2O (3×75 mL). The organic layer was collected, dried over Na_2SO_4, filtered, and concentrated under reduced pressure. The crude product was recrystallized from CH_2Cl_2/hexane afford a white solid (323 mg, 86% yield). ^{1}H NMR (500 MHz, $CDCl_3$), *δ* 7.94 (s, 2H), 7.72 (s, 4H).

Synthesis of **DBTS2O**: The synthetic process was similar to DBTS except for the change of starting materials. Pure DBTS2O was isolated as yellow solid with the yield of 72%. ^{1}H NMR (500 MHz, $CDCl_3$) *δ* 8.00 (s, 2H), 7.89 (d, *J* = 8.0 Hz, 2H), 7.72 (d, *J* = 8.1 Hz, 2H), 7.53 (d, *J* = 8.6 Hz, 4H), 7.31 (t, *J* = 8.1 Hz, 8H), 7.19–7.16 (m, 12H), 7.10 (t, *J* = 7.4 Hz, 4H); ^{13}C NMR (126 MHz, $CDCl_3$) *δ* 148.67, 147.27, 146.74, 136.10, 132.37, 129.45, 128.54, 128.06, 124.92, 123.59, 123.11, 122.52, 119.42; HRMS: *m*/*z:* $[M]^+$ calcd for $[C_{48}H_{34}N_2O_2S]^+$: 702.2341; found: 702.2344.

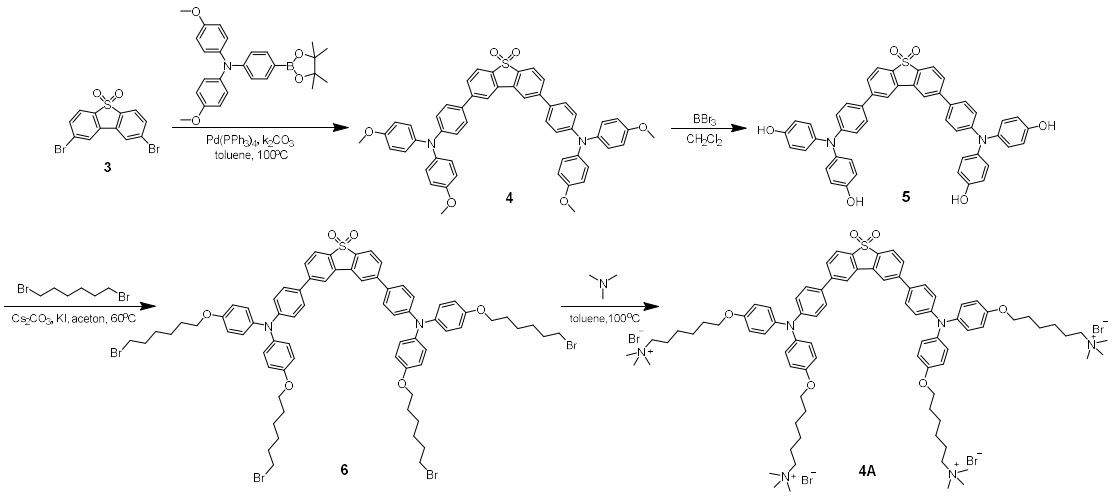

Scheme S4. Synthetic routes to 2OA.

Synthesis of **4**: The synthetic process was similar to DBTS except for the change of starting materials. Pure **4** was isolated as yellow solid with the yield of 70%. ^{1}H NMR (600 MHz, $CDCl_3$) δ 7.97 (s, 2H), 7.86 (d, J = 7.9 Hz, 2H), 7.69 (d, J = 7.9 Hz, 2H), 7.48 (d, J = 8.1 Hz, 4H), 7.14 (d, J = 8.2 Hz, 8H), 7.03 (d, J = 8.1 Hz, 4H), 6.90 (d, J = 8.3 Hz, 8H), 3.84 (s, 12H); ^{13}C NMR (151 MHz, $CDCl_3$) δ 156.34, 149.52, 146.86, 140.30, 135.77, 132.40, 130.35, 128.21, 127.84, 127.03, 122.42, 119.96, 119.10, 114.86, 55.53.

Synthesis of **5**: To a solution of **4** (116 mg, 0.14 mmol) in CH_2Cl_2 (12 mL) was added BBr_3 (2 mL, 2.8 mmol, 1.0 M in CH_2Cl_2) at 0 ºC. The mixture was stirred for 5 h at room temperature, and then saturated aq. $NaHCO_3$ (5 mL) was added to the solution. The reaction mixture was extracted with CH_2Cl_2 (50 mL), and the organic layer was washed with water and concentrated in vacuo. The crude product was recrystallized from CH_3OH/ ethyl acetate afford an atrovirens solid (65 mg, 60% yield). ^{1}H NMR (600 MHz, DMSO-d_6) δ 9.43 (s, 4H), 8.57 (s, 2H), 7.94 (d, J = 8.1 Hz, 2H), 7.84 (d, J = 8.2 Hz, 2H), 7.69 (d, J = 8.6 Hz, 4H), 7.01 (d, J = 8.5 Hz, 8H), 6.79–6.77 (m, 12H).

Synthesis of **6**: To a 50 mL round bottom flask was added **5** (50 mg, 0.065 mmol), 1,6-dibromohexane (159 mg, 0.65 mmol), Cs_2CO_3 (254 mg, 0.78 mmol) and KI (3.2 mg, 0.0195). The solids were placed under an atmosphere of N_2. Aceton (5 mL) was added via syringe. The reaction mixture was refluxed for 6 h at 60 °C. Then, the reaction was cooled to room temperature. The resulting slurry was separated from solid and liquid. The filter was washed with ethyl acetate (10 mL). The organic layer was collected, dried over Na_2SO_4, filtered, and concentrated under reduced pressure. The crude product was purified by silica gel column chromatography using petroleumether/ethyl acetate (*v*:*v*, 5:1) as an eluent to afford a yellow solid (49 mg, 53% yield). ^{1}H NMR (600 MHz, $CDCl_3$) δ 7.97 (s, 2H), 7.86 (d, J = 8.0 Hz, 2H), 7.69 (d, J = 8.0 Hz, 2H), 7.48 (d, J = 8.6 Hz, 4H), 7.12 (d, J = 8.8 Hz, 8H), 7.02 (d, J = 8.6 Hz, 4H), 6.88 (d, J = 8.9 Hz, 8H), 3.98 (t, J = 6.2 Hz, 8H), 3.46 (t, J = 6.7 Hz, 8H), 1.94 (t, J = 6.7 Hz, 8H), 1.83 (t, J = 6.4 Hz, 8H), 1.55 (t, J = 3.5 Hz, 16H); ^{13}C NMR (151 MHz, $CDCl_3$) δ 155.83, 149.50, 146.85, 140.17, 135.73, 132.39, 130.27, 128.21, 127.83, 127.05, 122.40, 119.91, 119.09, 115.41, 68.02, 33.83, 32.71, 29.18, 27.96, 25.36.

Synthesis of **2OA**: To a 50 mL pressure vial was added **6** (48 mg, 0.034 mmol), trimethylamine (16 mg, 0.27 mmol) and toluene (3 mL). The resulting solution was stirred under N_2 atmosphere at 100 °C overnight. Then, the reaction was cooled to room temperature. The solvent was

evaporated under reduced pressure. The crude solid was washed with ethyl acetate. Pure 2OA was obtained as yellow solid (47 mg, 84% yield). ^{1}H NMR (600 MHz, DMSO-d_6) δ 8.61 (s, 2H), 7.98 (d, J = 8.0 Hz, 2H), 7.86 (d, J = 8.2 Hz, 2H), 7.75 (d, J = 8.4 Hz, 4H), 7.09 (d, J = 8.7 Hz, 8H), 6.96 (d, J = 8.6 Hz, 8H), 6.87 (d, J = 8.5 Hz, 4H), 3.98 (t, J = 6.1 Hz, 8H), 3.31–3.09 (m, 8H), 3.07 (s, 36H), 1.78–1.70 (m, 16H), 1.52–1.47 (m, 8H), 1.38–1.33 (m, 8H); ^{13}C NMR (151 MHz, $CDCl_3$) δ 156.02, 149.61, 146.39, 139.96, 135.54, 132.35, 129.66, 128.61, 128.39, 127.56, 122.80, 120.44, 119.27, 116.03, 68.00, 65.72, 52.65, 28.96, 25.99, 25.59, 22.50; HRMS: *m*/*z:* $[M]^{4+}$ calcd for $[C_{84}H_{114}N_6O_6S]^{4+}$: 333.7125; found: 333.7133.

Supplementary figures

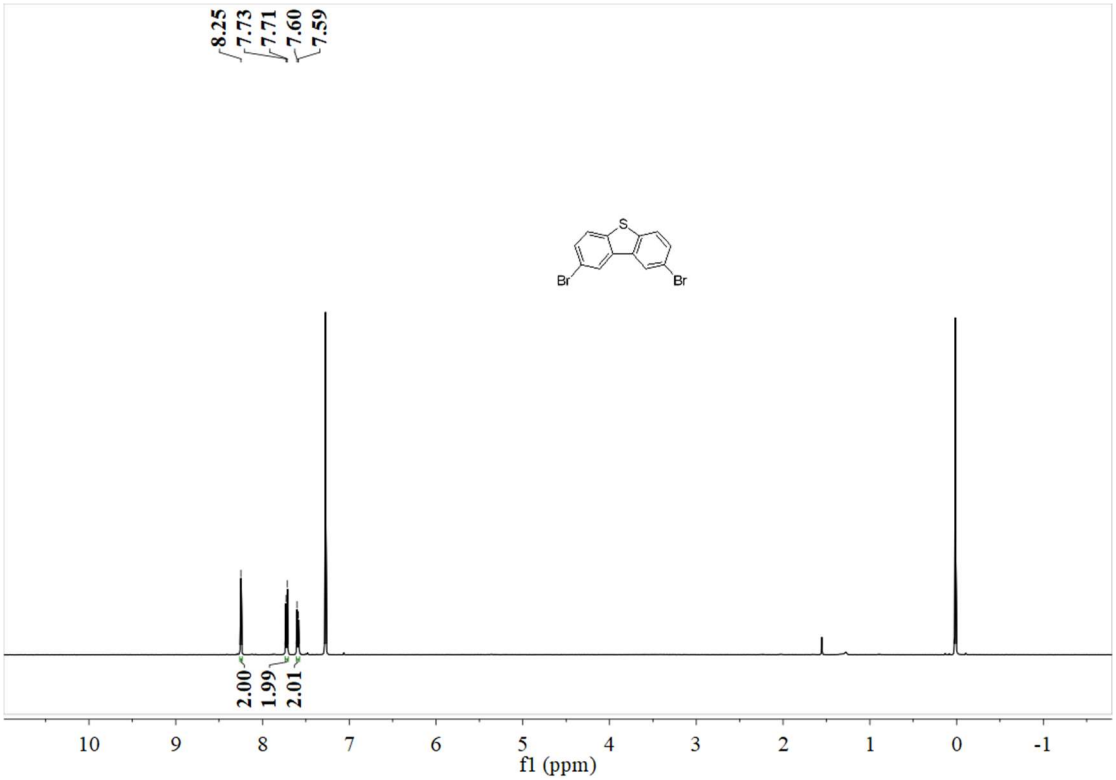

Figure S1. ^{1}H NMR spectrum of compound **1** in $CDCl_3$.

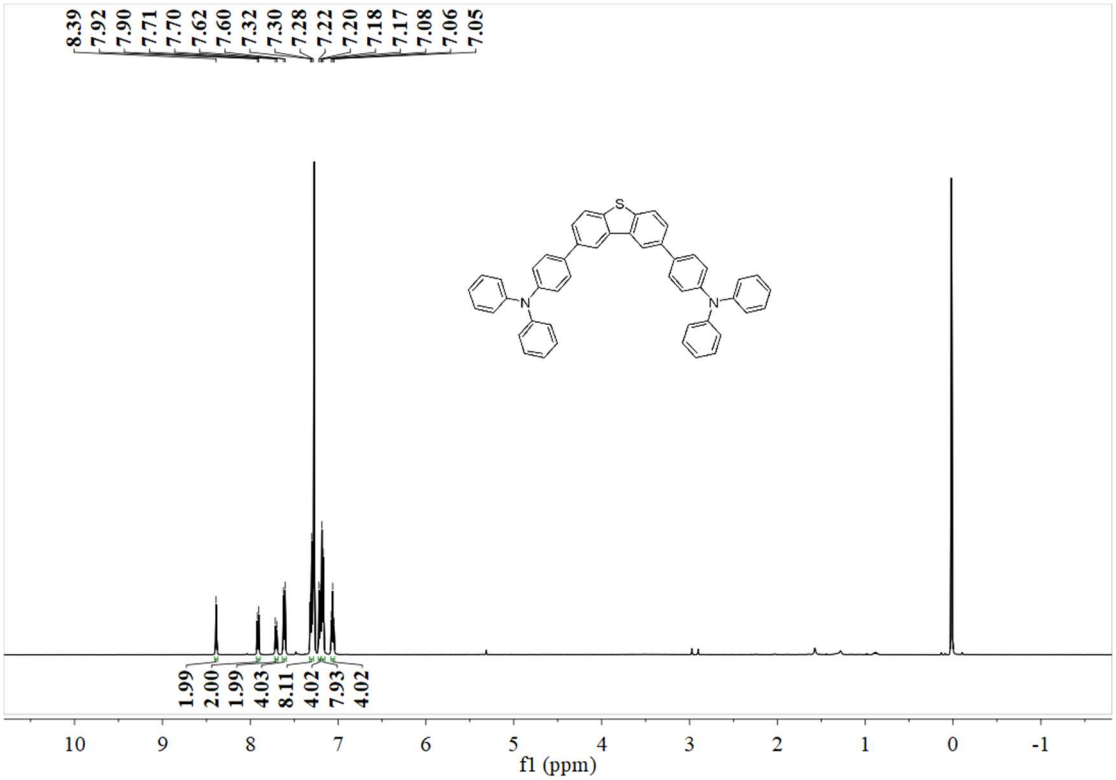

Figure S2. ^{1}H NMR spectrum of DBTS in $CDCl_3$.

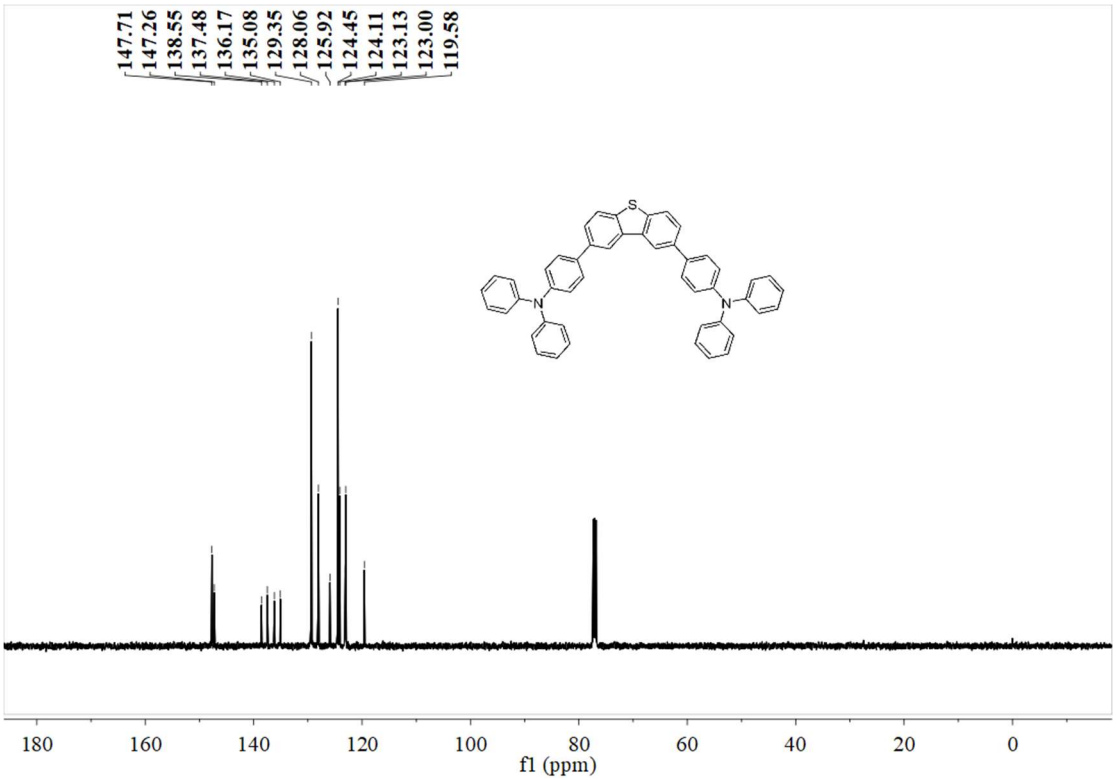

Figure S3. ^{13}C NMR spectrum of DBTS in $CDCl_3$.

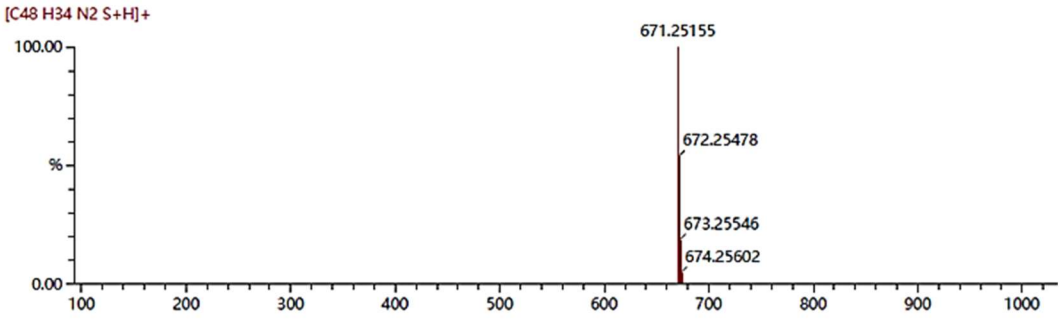

Figure S4. HRMS spectrum of DBTS.

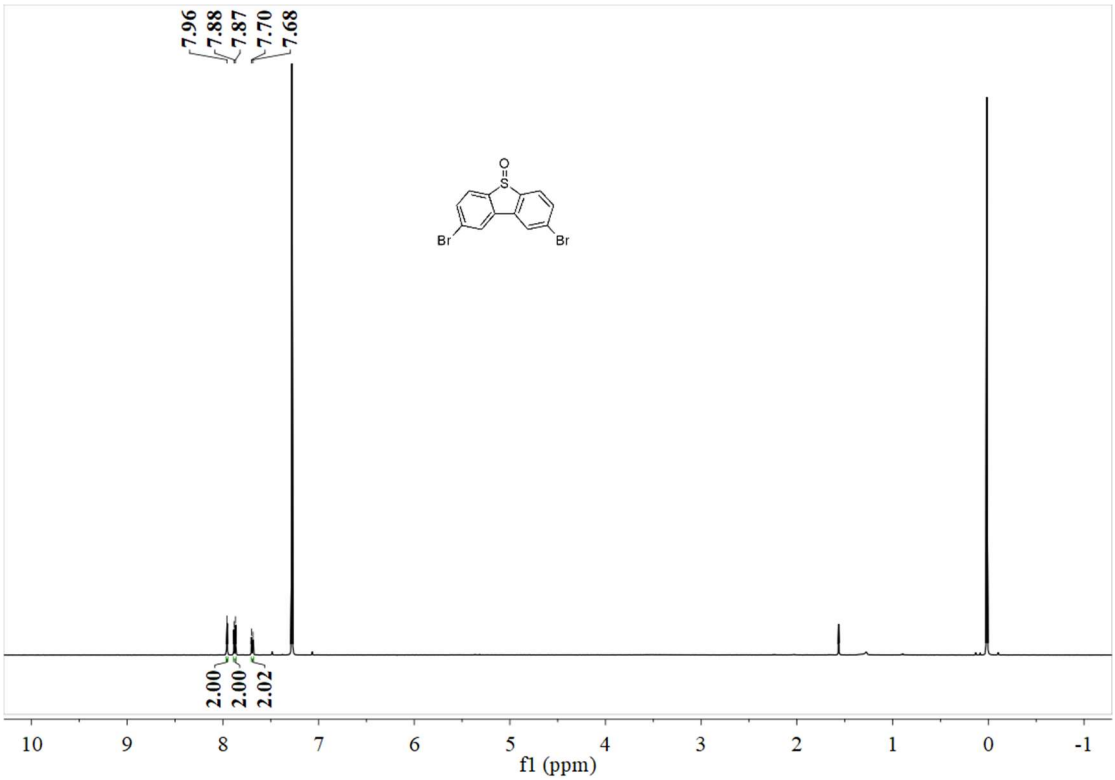

Figure S5. ^{1}H NMR spectrum of compound **2** in $CDCl_3$.

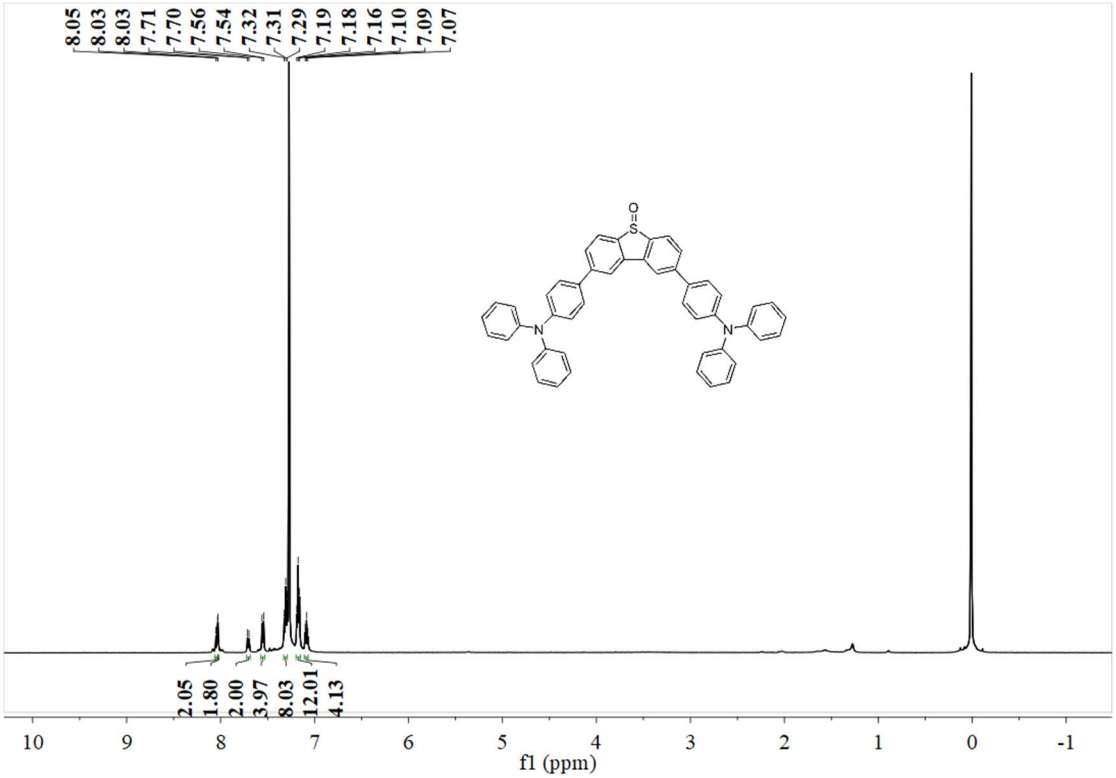

Figure S6. ^{1}H NMR spectrum of DBTSO in $CDCl_3$.

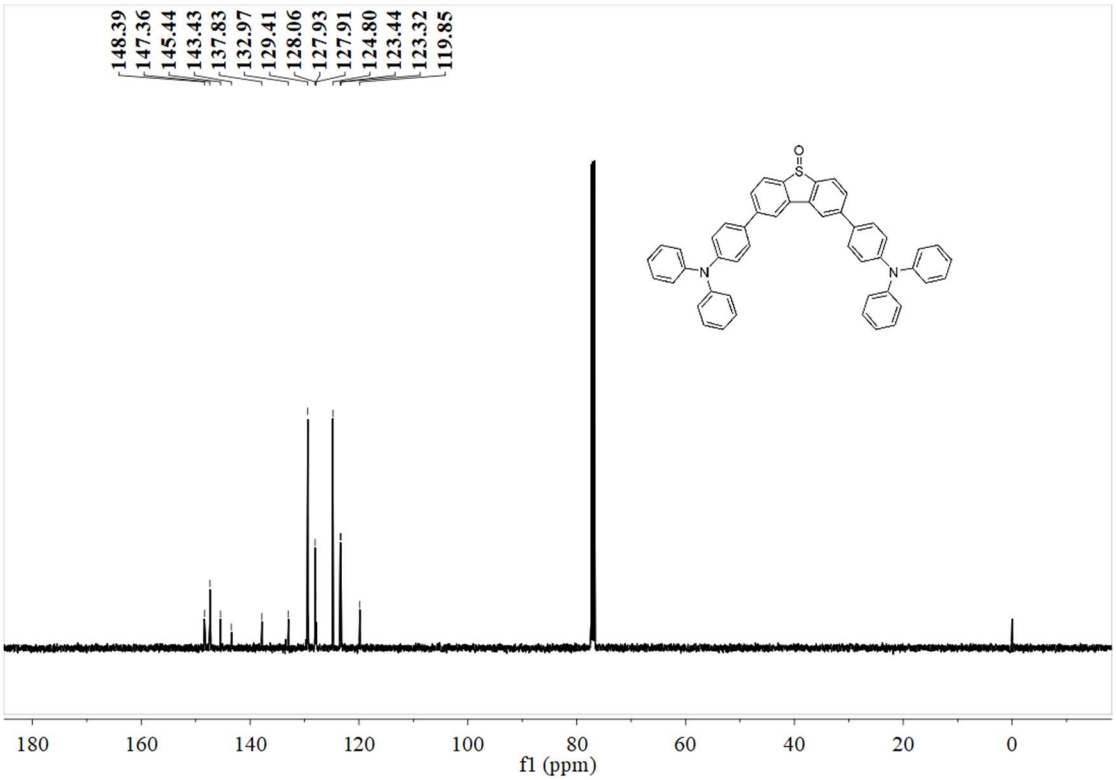

Figure S7. ^{13}C NMR spectrum of DBTSO in $CDCl_3$.

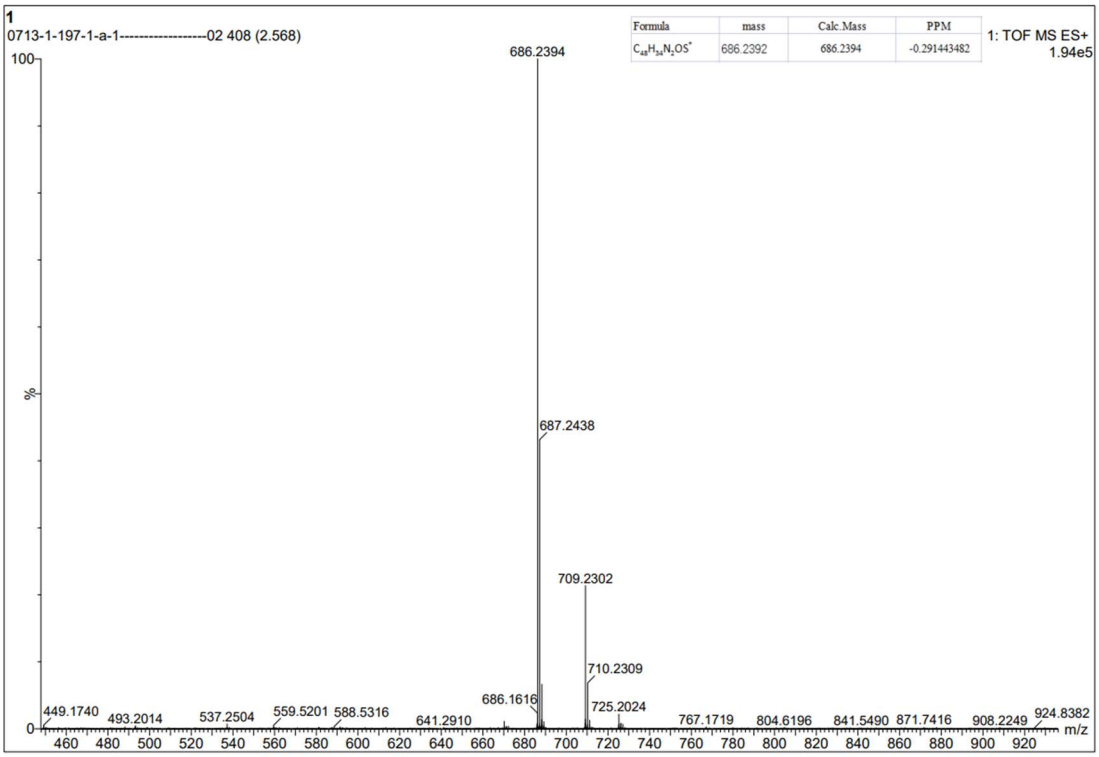

Figure S8. HRMS spectrum of DBTSO.

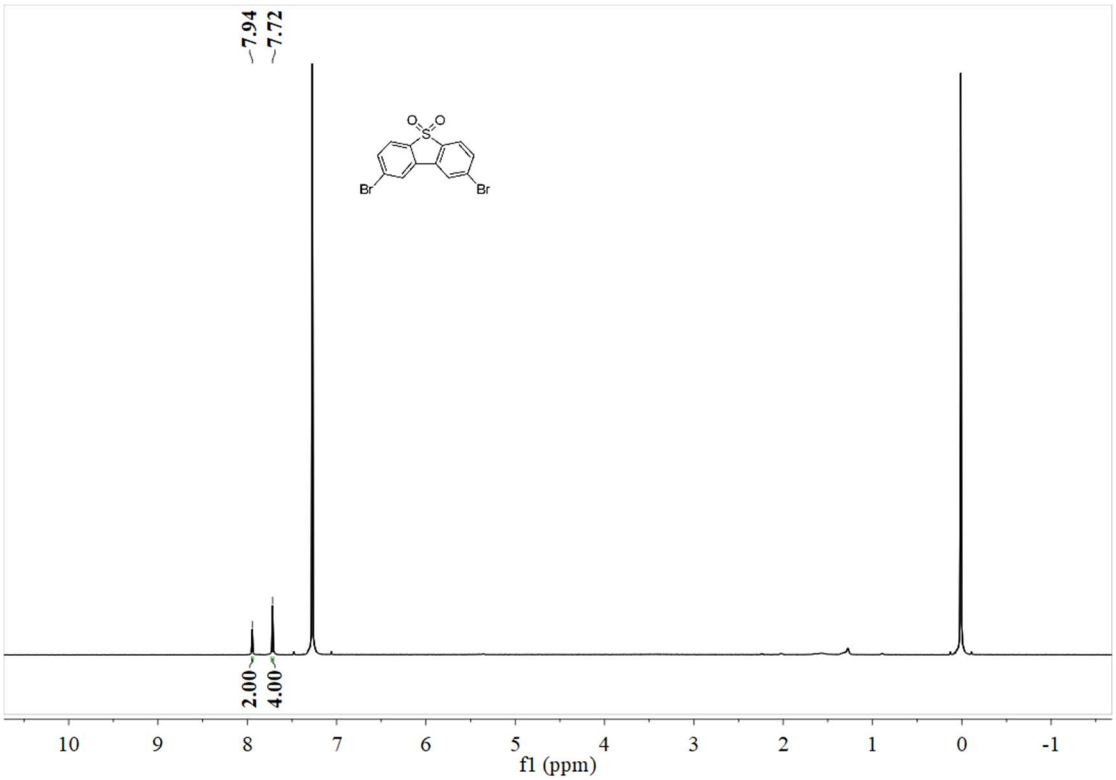

Figure S9. ^{1}H NMR spectrum of compound **3** in $CDCl_3$.

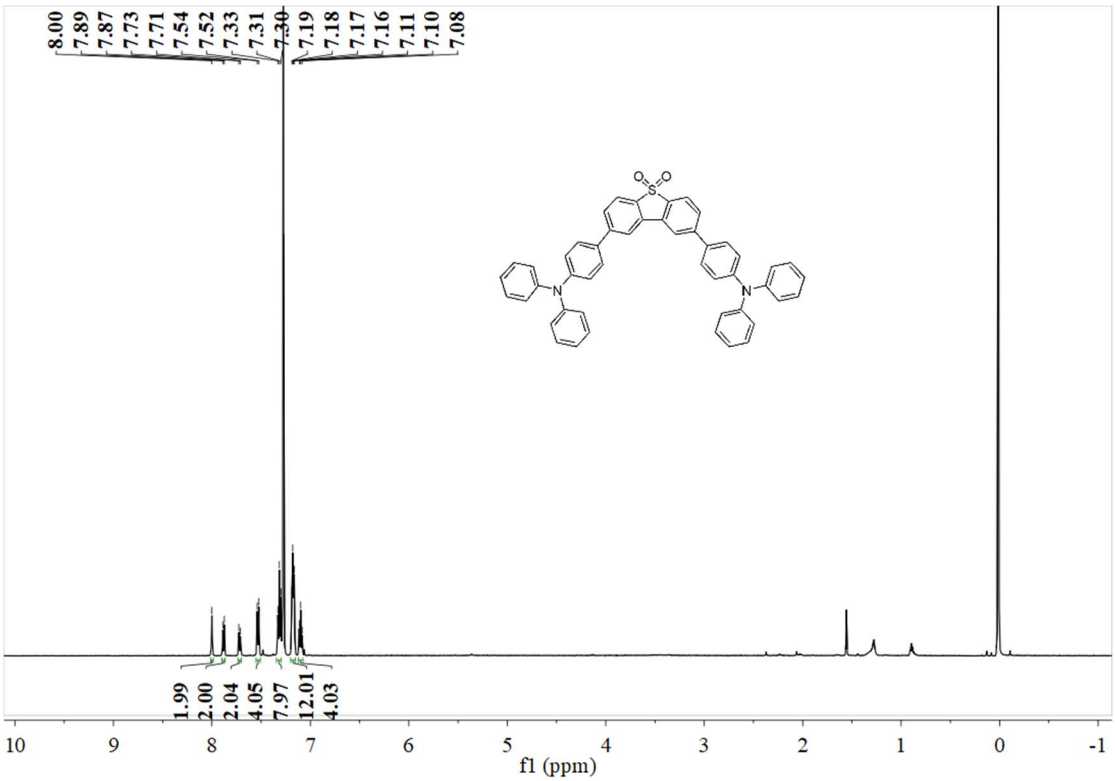

Figure S10. ^{1}H NMR spectrum of DBTS2O in $CDCl_3$.

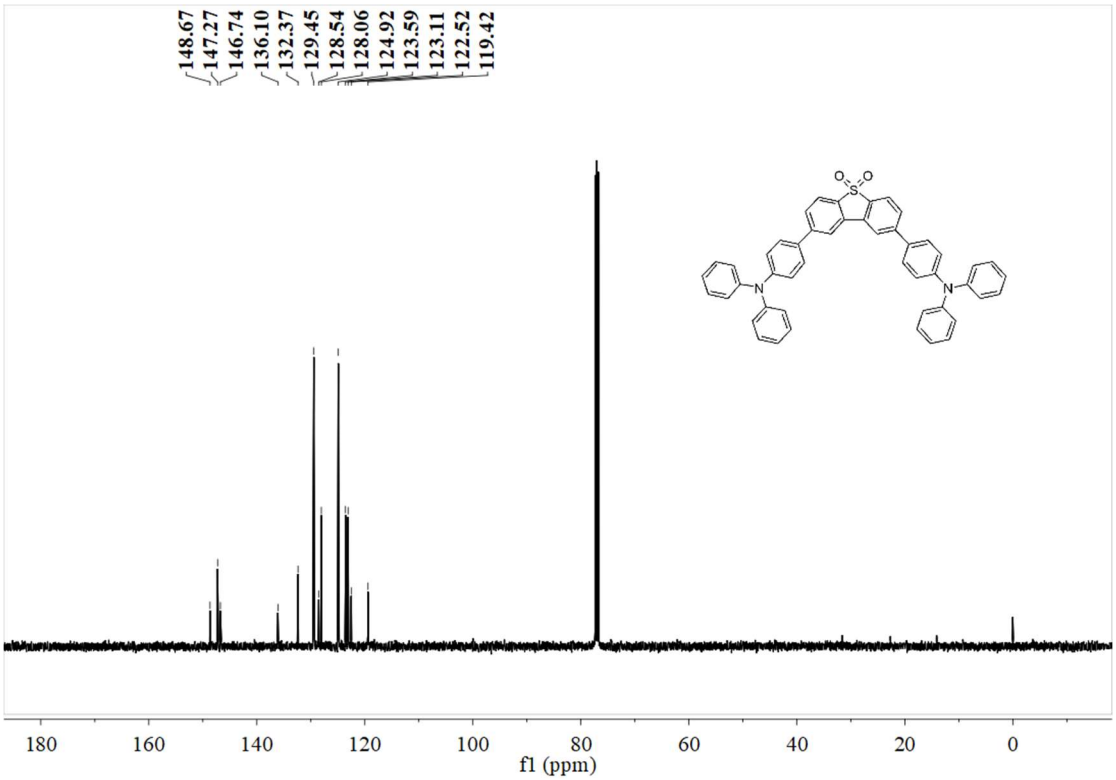

Figure S11. ^{13}C NMR spectrum of DBTS2O in $CDCl_3$.

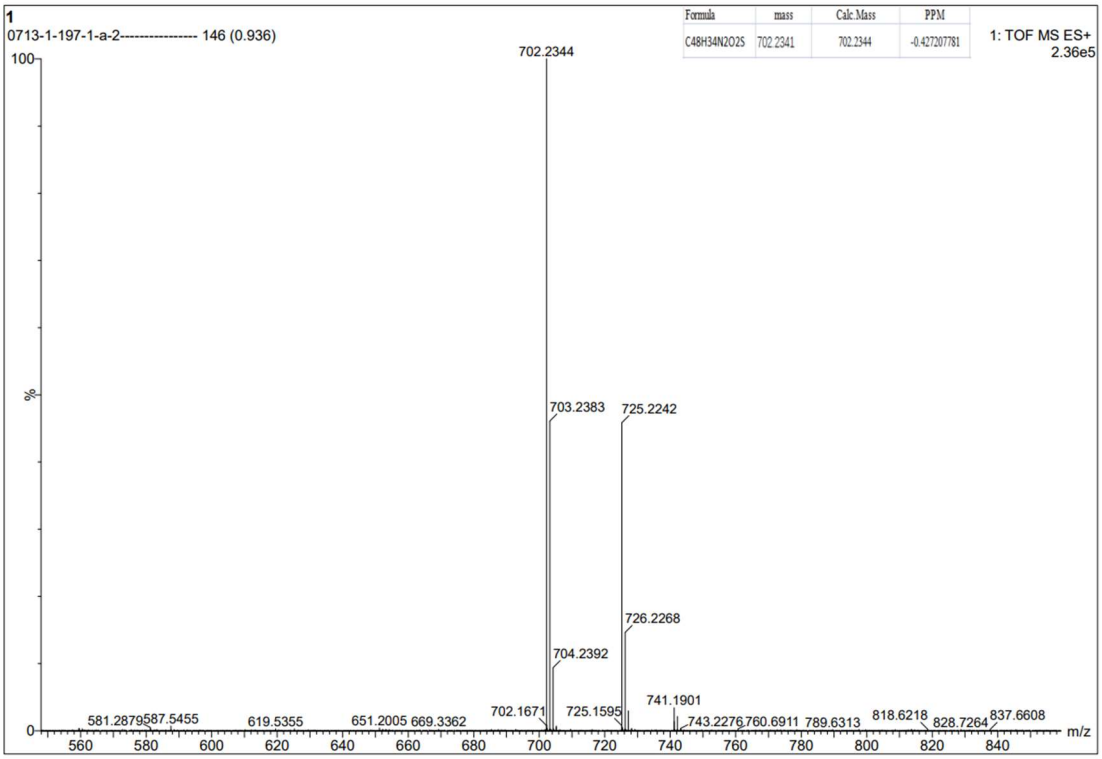

Figure S12. HRMS spectrum of DBTS2O.

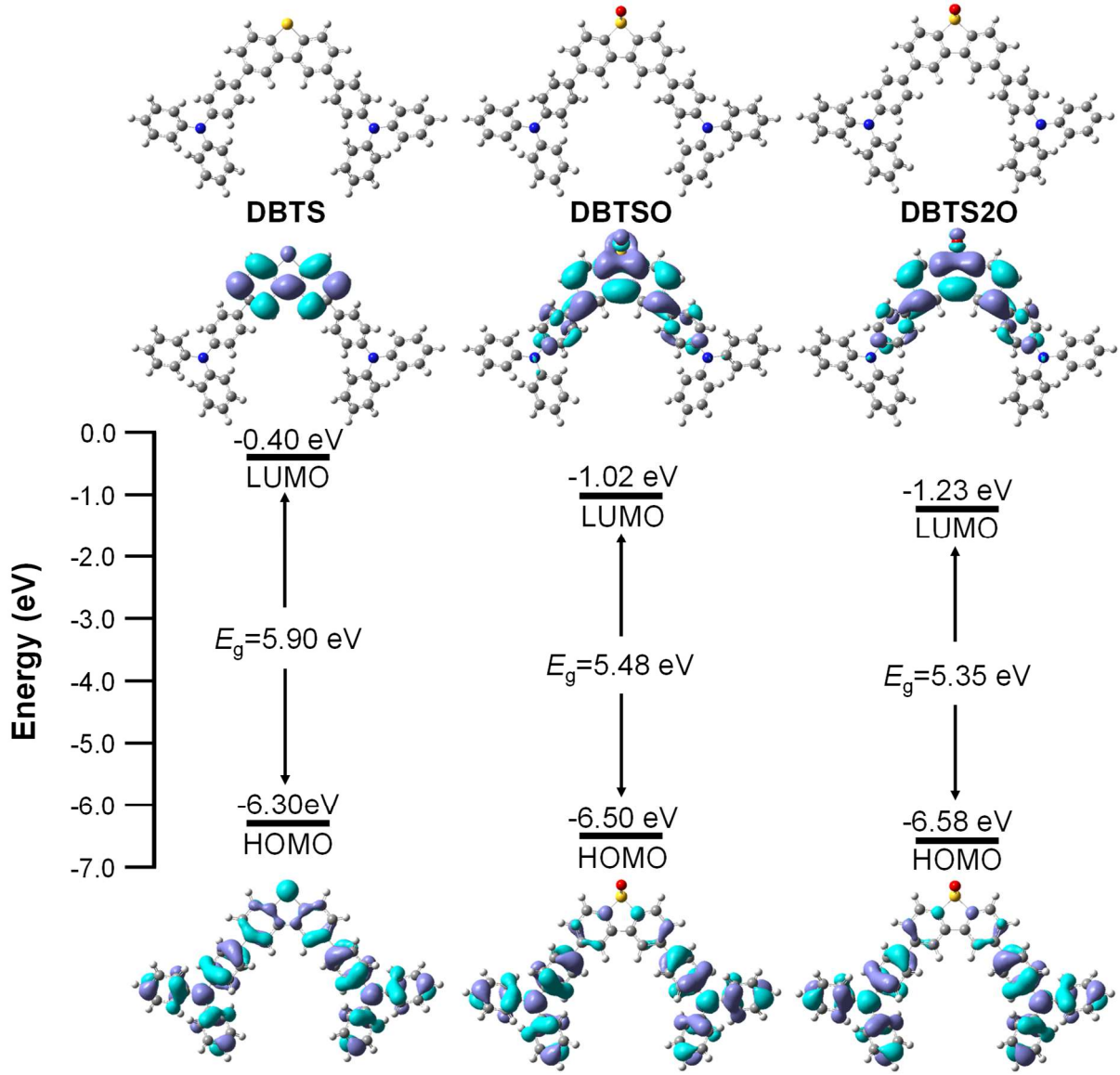

Figure S13. The HOMO and LUMO electron cloud distribution of DBTS, DBTSO and DBTS2O.

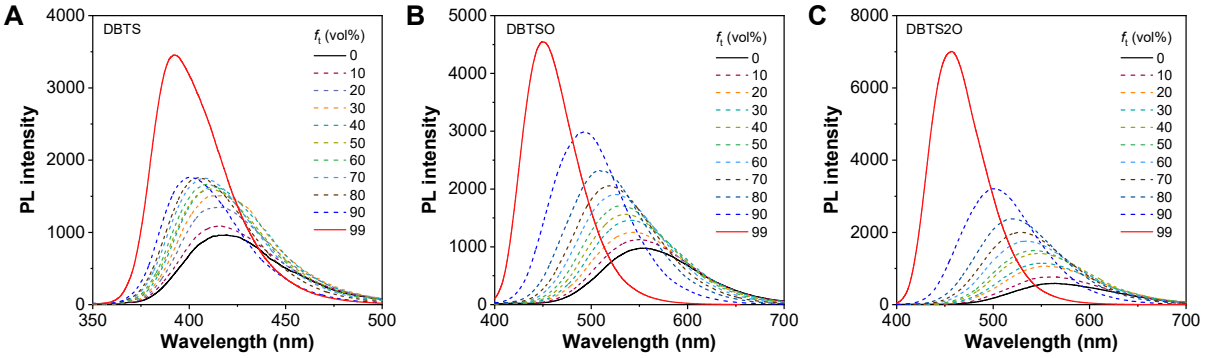

Figure S14. The fluorescence spectra of (A) DBTS, (B) DBTSO and (C) DBTS2O in DMSO/toluene mixtures with different toluene fractions (f_t).

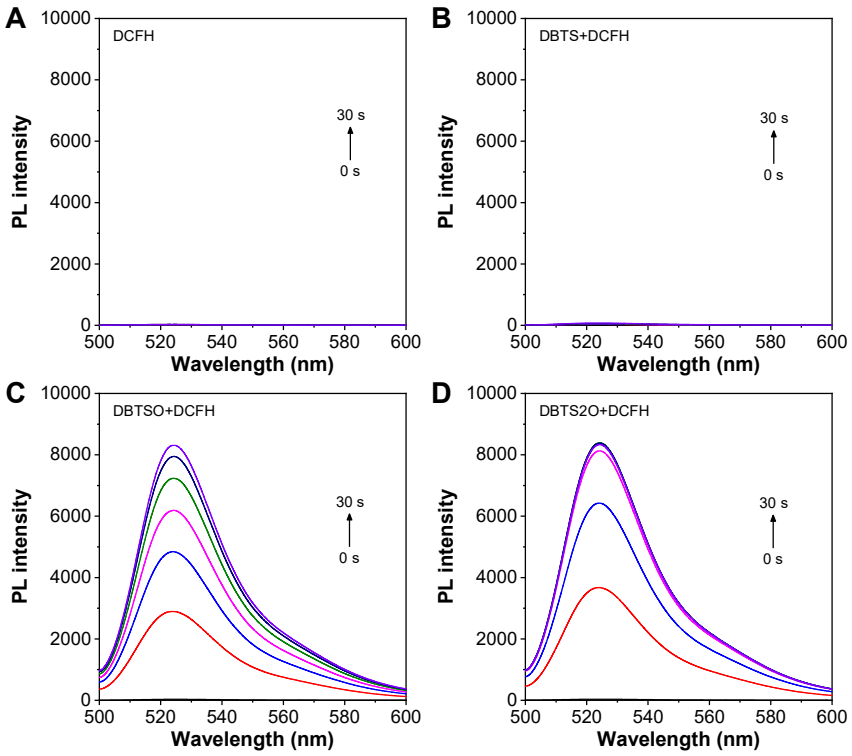

Figure S15. The fluorescence spectra changes of DCFH as the indicator for ROS detection. (A) DCFH alone, (B) DBTS+DCFH, (C) DBTSO+DCFH and (D) DBTS2O+DCFH after irradiated to white light (100 mW cm^{-2}) with different time. The concentration of DBTS, DBTSO and DBTS2O is 5 μM.

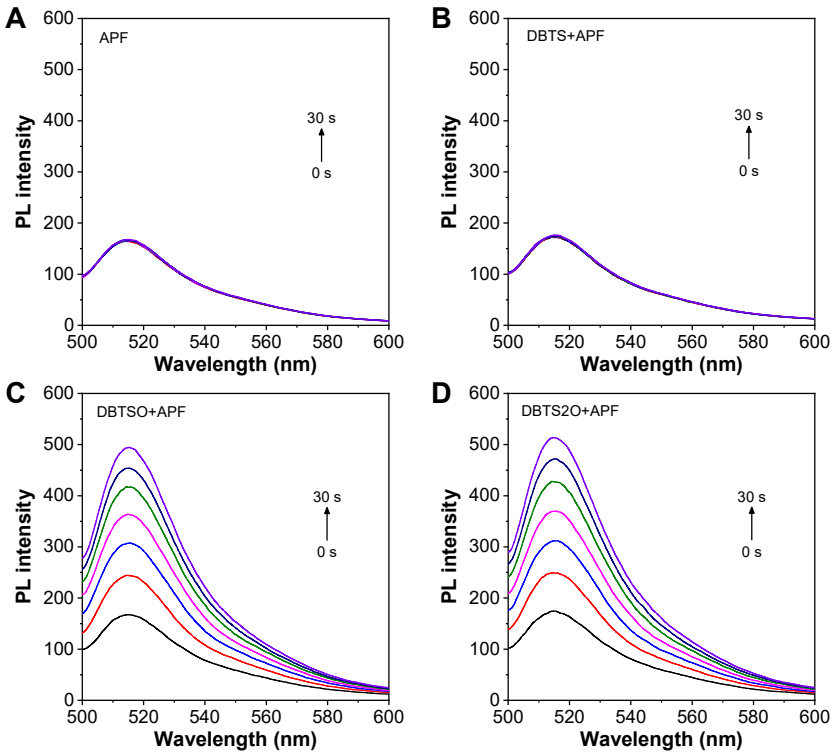

Figure S16. The fluorescence spectra changes of APF as the indicator for ROS detection. (A) APF alone, (B) DBTS+APF, (C) DBTSO+APF and (D) DBTS2O+APF after irradiated to white light (100 mW cm^{-2}) with different time. The concentration of DBTS, DBTSO and DBTS2O is 5 μM.

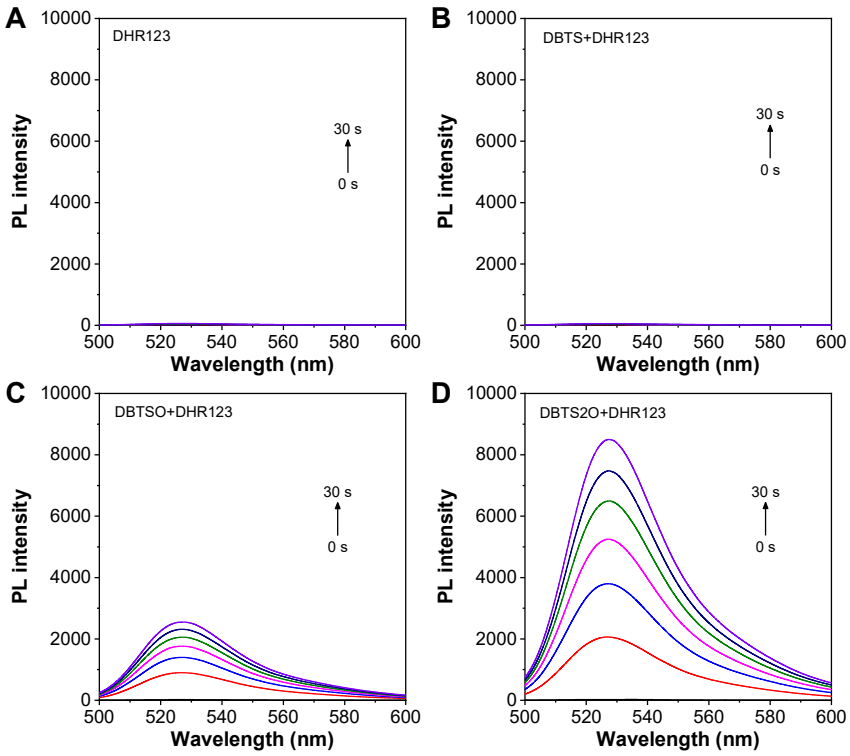

Figure S17. The fluorescence spectra changes of DHR123 as the indicator for ROS detection. (A) DHR123 alone, (B) DBTS+DHR123, (C) DBTSO+DHR123 and (D) DBTS2O+DHR123 after irradiated to white light (100 mW cm^{-2}) with different time. The concentration of DBTS, DBTSO and DBTS2O is 5 μM.

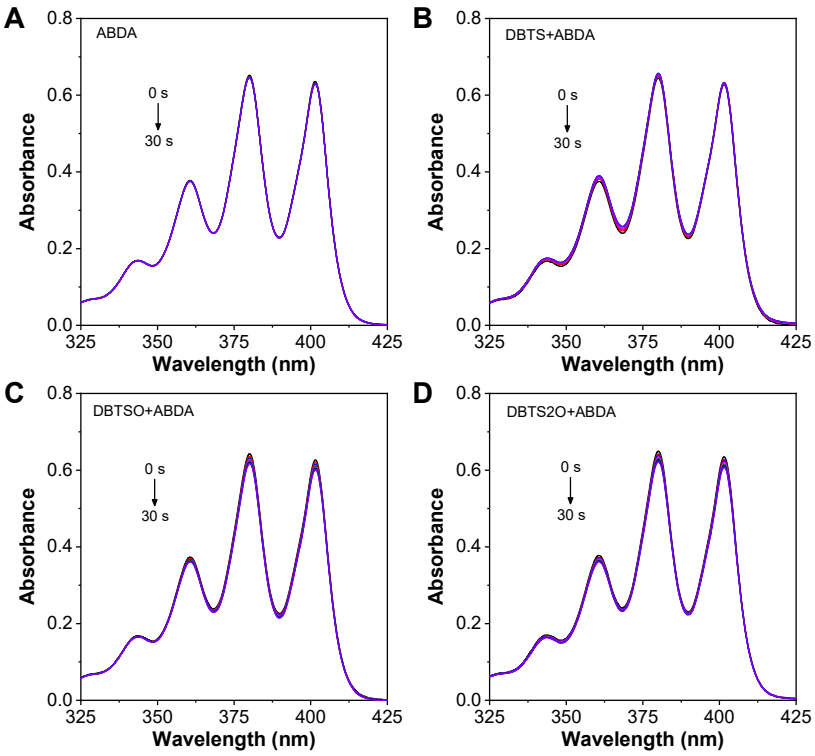

Figure S18. The fluorescence spectra changes of ABDA as the indicator for ROS detection. (A) ABDA alone, (B) DBTS+ABDA, (C) DBTSO+ABDA and (D) DBTS2O+ABDA after irradiated to white light (100 mW cm^{-2}) with different time. The concentration of DBTS, DBTSO and DBTS2O is 5 μM.

Table S1. Crystallographic and structural refinement data of DBTS, DBTSO and DBTS2O.

Name	DBTS	DBTSO	DBTS2O
Empirical formula	$C_{48}H_{34}N_2S$	$C_{48}H_{34}N_2OS$	$C_{48}H_{34}N_2O_2S$
Formula weight	670.83	686.83	702.83
Temperature (K)	150.00(10)	149.99(10)	100.00(10)
Wavelength (Å)	0.71073	0.71073	0.71073
Crystal system	monoclinic	monoclinic	monoclinic
Space group	C2/c	Cc	C2/c
a (Å)	14.2638(10)	14.3196(16)	14.6095(11)
b (Å)	17.9124(12)	17.8821(17)	17.9909(12)
c (Å)	14.1231(10)	14.0725(16)	14.0147(10)
α (°)	90	90	90
β (°)	105.354(8)	104.757(12)	104.842(7)
γ (°)	90	90	90
Volume (Å^3)	3479.6(4)	3484.6(7)	3560.7(5)
Z	4	4	4
Density (g/cm^3)	1.281	1.309	1.311
F(000)	1408.0	1440.0	1472.0
h_{max}, k_{max}, l_{max}	16, 21, 16	17, 21, 16	17, 21, 16
CCDC Number	2325250	2325253	2325255

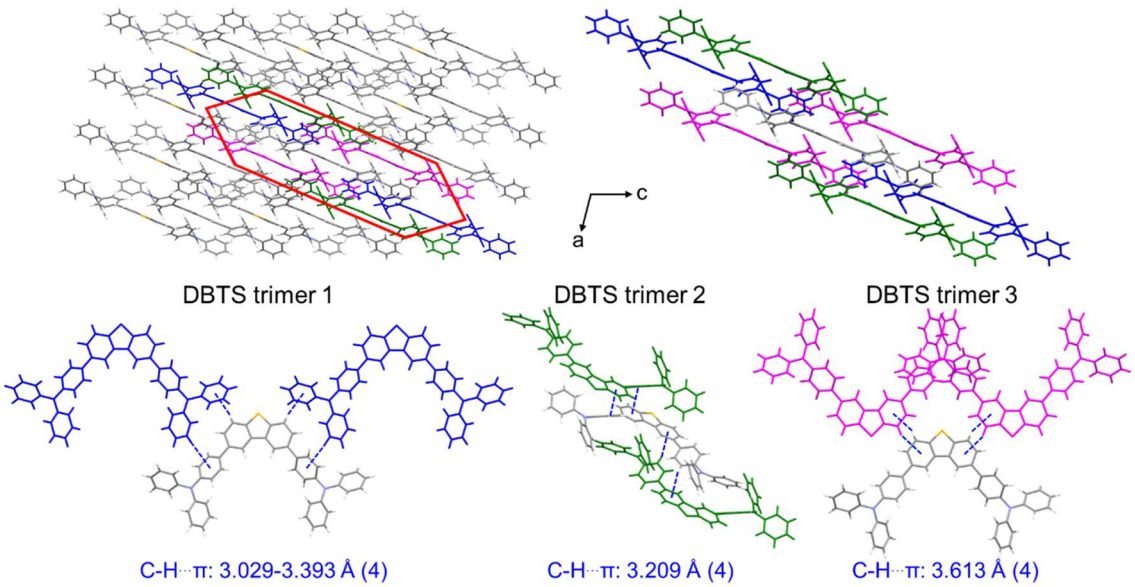

Figure S19. Molecular packing of DBTS crystal from the b direction and intermolecular interactions of DBTS trimers.

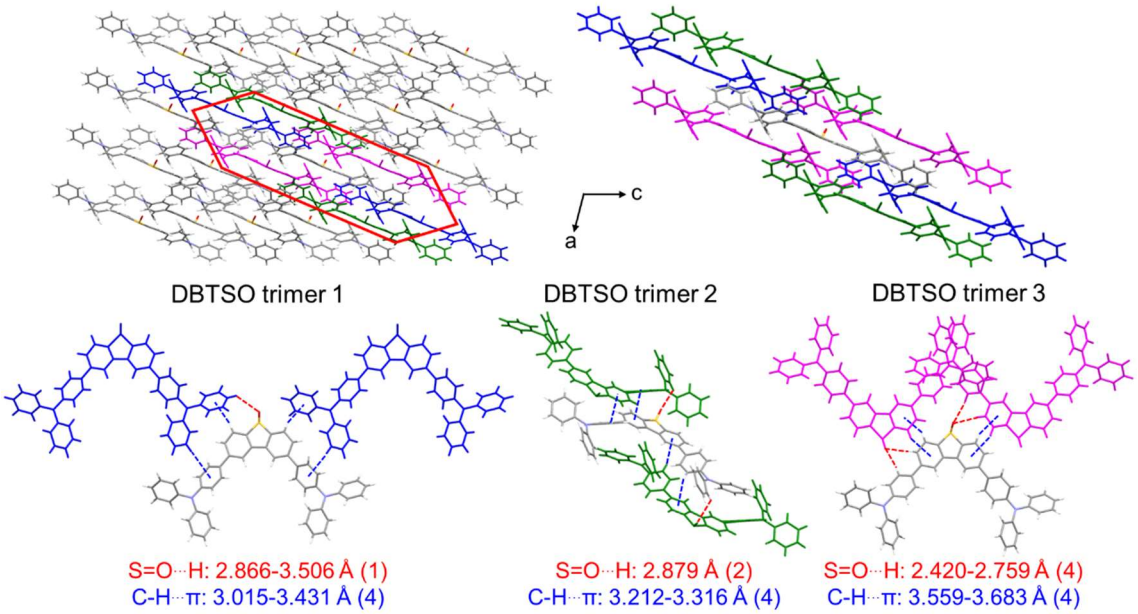

Figure S20. Molecular packing of DBTSO crystal from the b direction and intermolecular interactions of DBTSO trimers.

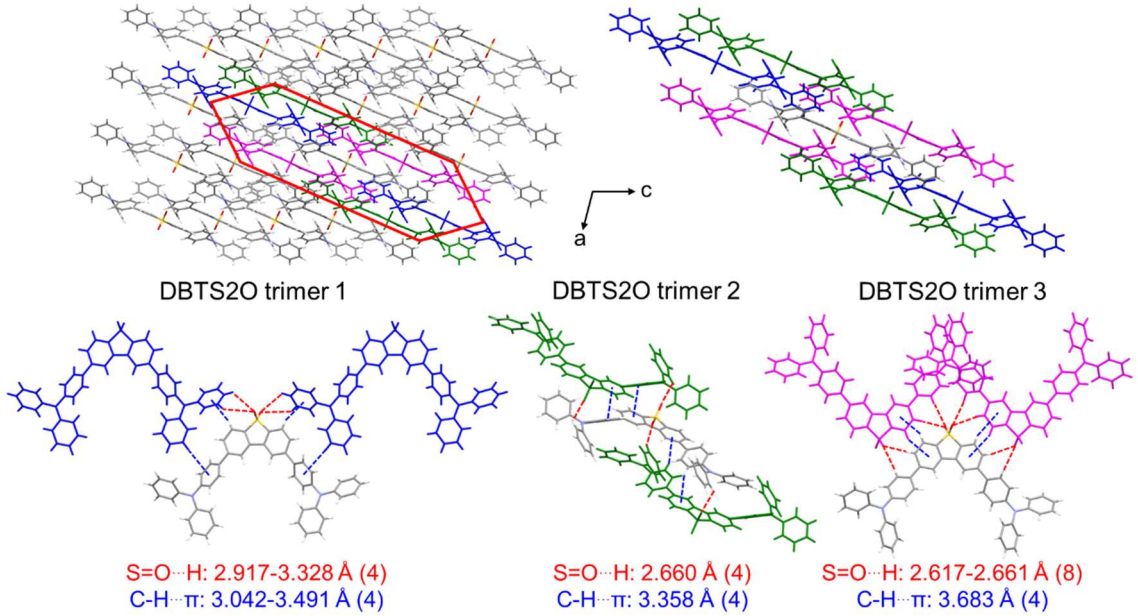

Figure S21. Molecular packing of DBTS2O crystal from the b direction and intermolecular interactions of DBTS2O trimers.

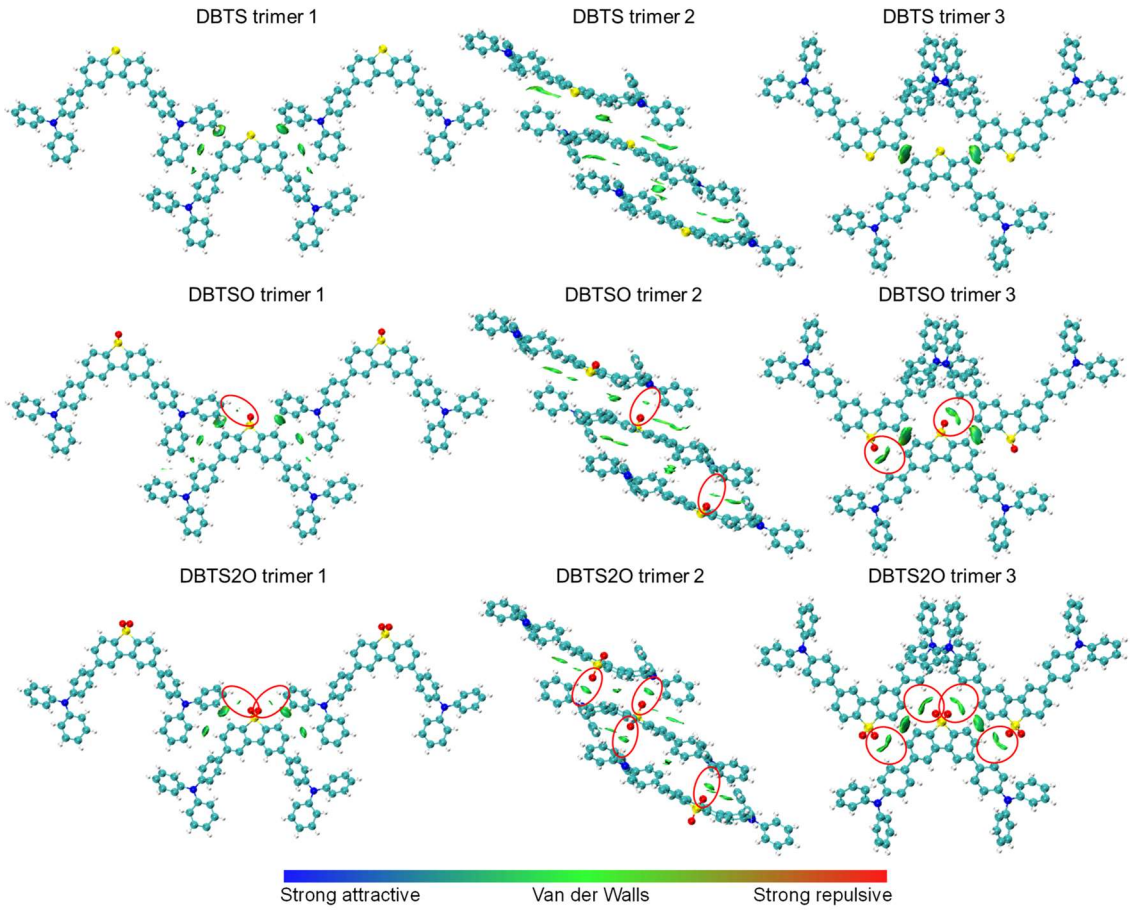

Figure S22. The visualized isosurfaces of the IGM analysis for trimers in DBTS, DBTSO and DBTS2O (δg^{inter} = 0.007).

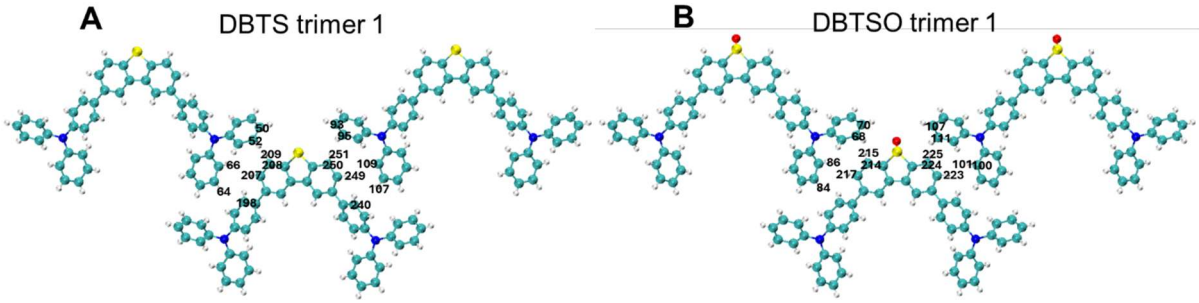

Atomic pair	Delta-g index	Percentage contribution
66 207	0.100622	1.72 %
109 249	0.100622	1.72 %
52 209	0.088992	1.52 %
95 251	0.088991	1.52 %
50 209	0.077691	1.33 %
93 251	0.077691	1.33 %
52 208	0.076182	1.30 %
95 250	0.076182	1.30 %
107 240	0.070809	1.21 %
64 198	0.070809	1.21 %

Atomic pair	Delta-g index	Percentage contribution
101 223	0.101546	1.70 %
68 215	0.095952	1.61 %
86 217	0.091379	1.53 %
70 215	0.084631	1.42 %
111 225	0.080533	1.35 %
68 214	0.077817	1.30 %
107 225	0.076275	1.28 %
111 224	0.073594	1.23 %
100 223	0.072431	1.21 %
84 205	0.070111	1.17 %

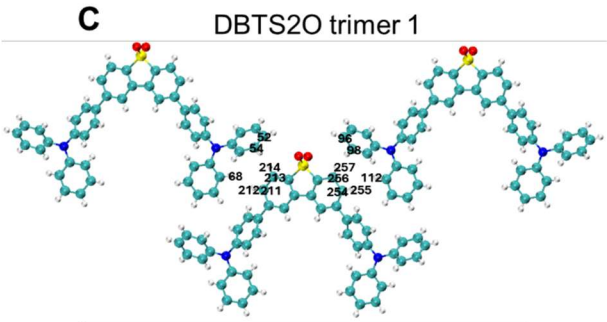

Atomic pair	Delta-g index	Percentage contribution
112 255	0.097890	1.68 %
68 212	0.097890	1.68 %
54 214	0.084457	1.45 %
98 257	0.084457	1.45 %
96 257	0.077246	1.32 %
52 214	0.077246	1.32 %
54 213	0.072712	1.25 %
98 256	0.072712	1.25 %
68 211	0.067040	1.15 %
112 254	0.067040	1.15 %

Figure S23. The contribution of ten atomic pairs with the largest percentage to intermolecular interactions of trimer 1 in (A) DBTS, (B) DBTSO and (C) DBTS2O.

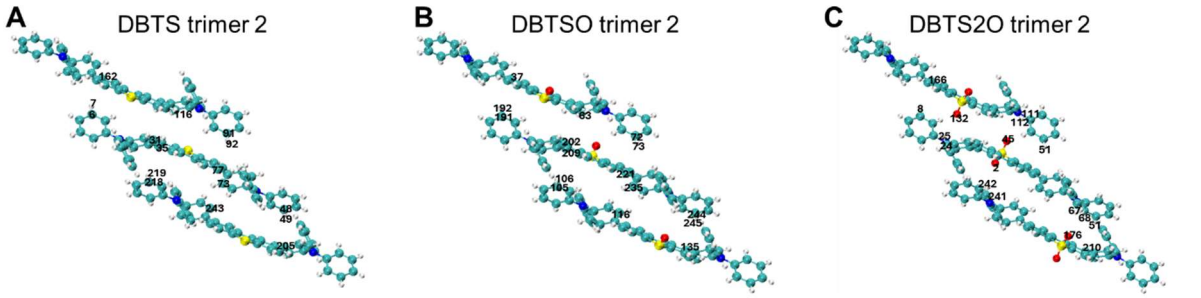

Atomic pair	Delta-g index	Percentage contribution
31 116	0.077660	0.51 %
73 243	0.077660	0.51 %
6 162	0.068614	0.45 %
48 205	0.068614	0.45 %
77 91	0.068583	0.45 %
35 218	0.068583	0.45 %
49 205	0.065174	0.42 %
7 162	0.065174	0.42 %
35 219	0.065136	0.42 %
77 92	0.065136	0.42 %

Atomic pair	Delta-g index	Percentage contribution
63 202	0.072583	0.48 %
116 235	0.072567	0.48 %
135 244	0.069421	0.45 %
72 221	0.069388	0.45 %
37 191	0.065559	0.43 %
105 209	0.065515	0.43 %
135 245	0.065376	0.43 %
73 221	0.065338	0.43 %
37 192	0.064003	0.42 %
106 209	0.063961	0.42 %

Atomic pair	Delta-g index	Percentage contribution
2 242	0.083056	0.59 %
45 112	0.083056	0.59 %
25 132	0.083036	0.59 %
68 176	0.083036	0.59 %
2 241	0.072785	0.51 %
45 111	0.072785	0.51 %
67 176	0.072769	0.51 %
24 132	0.072769	0.51 %
8 166	0.064863	0.46 %
51 210	0.064863	0.46 %

Figure S24. The contribution of ten atomic pairs with the largest percentage to intermolecular interactions of trimer 2 in (A) DBTS, (B) DBTSO and (C) DBTS2O.

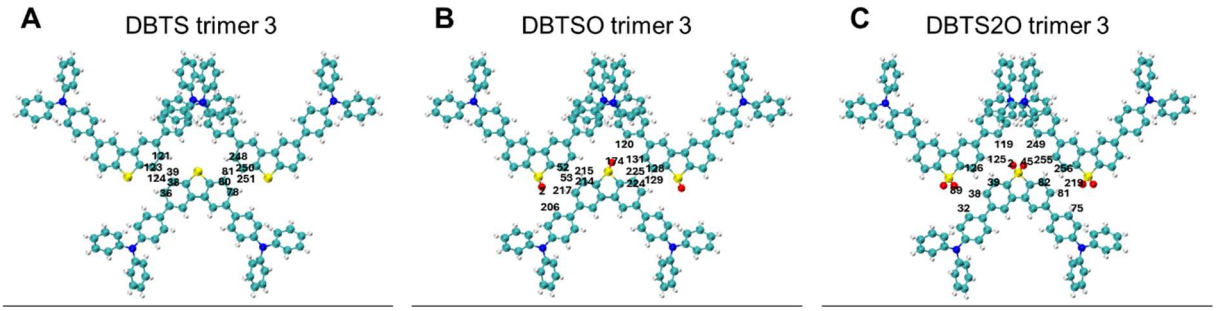

Atomic pair	Delta-g index	Percentage contribution
80 250	0.091779	2.98 %
38 123	0.091779	2.98 %
80 251	0.077426	2.52 %
38 124	0.077426	2.52 %
39 123	0.077412	2.52 %
81 250	0.077412	2.52 %
78 251	0.057359	1.86 %
36 124	0.057359	1.86 %
81 248	0.057298	1.86 %
39 121	0.057298	1.86 %

Atomic pair	Delta-g index	Percentage contribution
120 174	0.119522	3.02 %
2 206	0.119510	3.02 %
128 224	0.090597	2.29 %
52 214	0.090589	2.29 %
53 214	0.082846	2.09 %
128 225	0.082841	2.09 %
129 224	0.072604	1.83 %
52 215	0.072587	1.83 %
131 174	0.070759	1.79 %
2 217	0.070753	1.79 %

Atomic pair	Delta-g index	Percentage contribution
81 219	0.089063	2.14 %
38 89	0.089063	2.14 %
2 125	0.089045	2.14 %
45 255	0.089044	2.14 %
39 126	0.083530	2.01 %
82 256	0.083530	2.01 %
75 219	0.083172	2.00 %
32 89	0.083172	2.00 %
45 249	0.083112	2.00 %
2 119	0.083112	2.00 %

Figure S25. The contribution of ten atomic pairs with the largest percentage to intermolecular interactions of trimer 3 in (A) DBTS, (B) DBTSO and (C) DBTS2O.

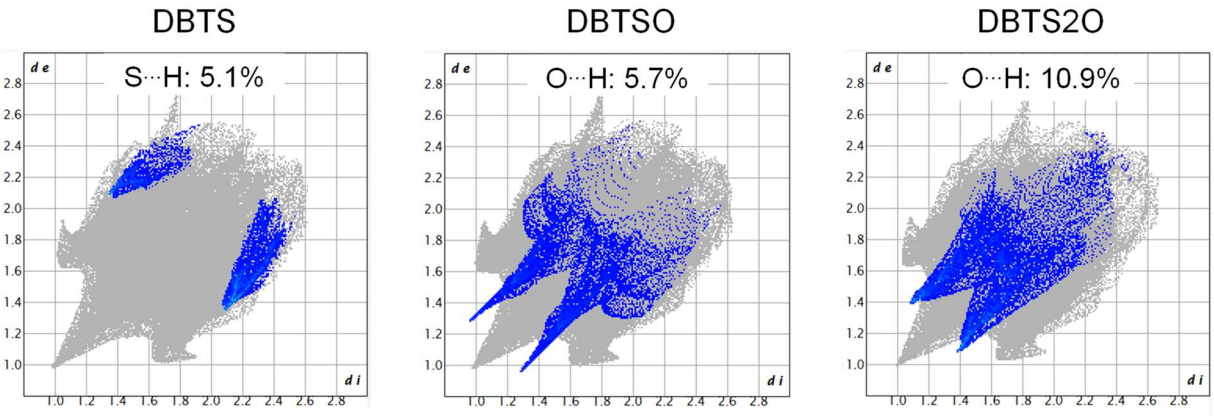

Figure S26. Fingerprint plot of intermolecular S···H interaction for DBTS, intermolecular O···H interaction for DBTSO and intermolecular O···H interaction for DBTS2O.

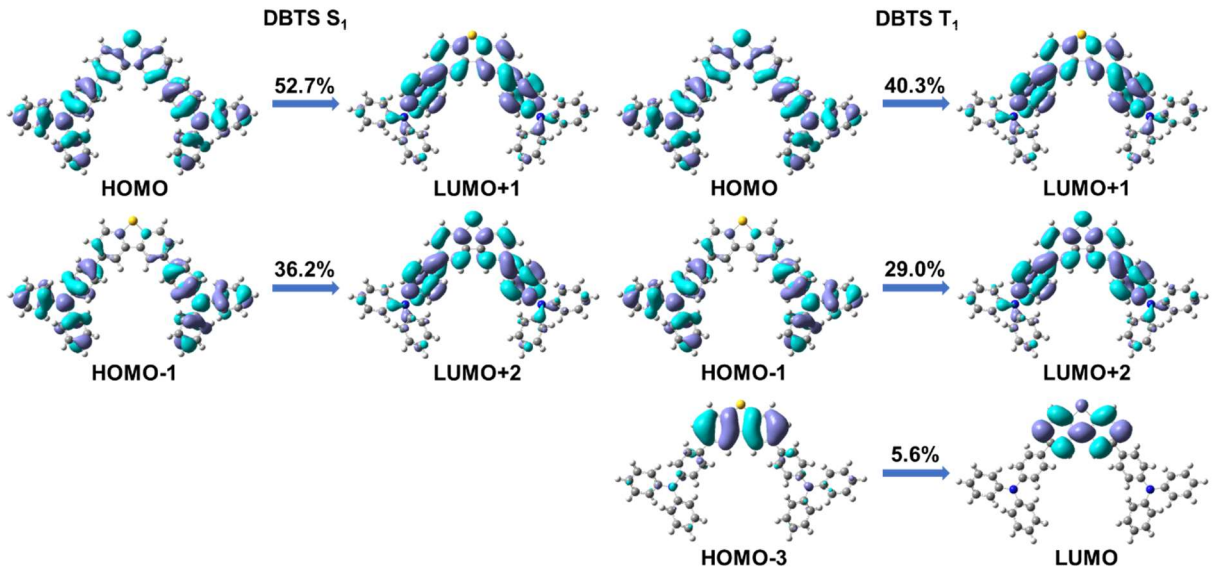

Figure S27. The molecular orbitals of corresponding transition configurations for S_1 and T_1 state of DBTS.

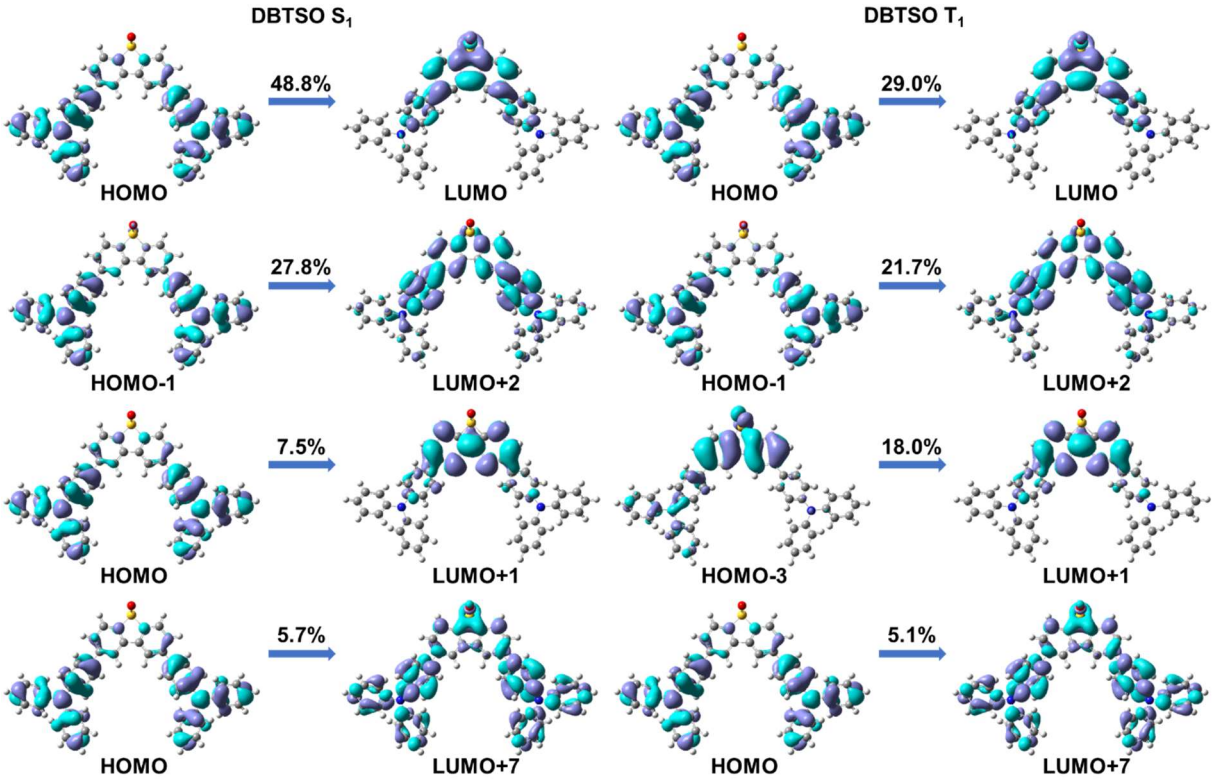

Figure S28. The molecular orbitals of corresponding transition configurations for S_1 and T_1 state of DBTSO.

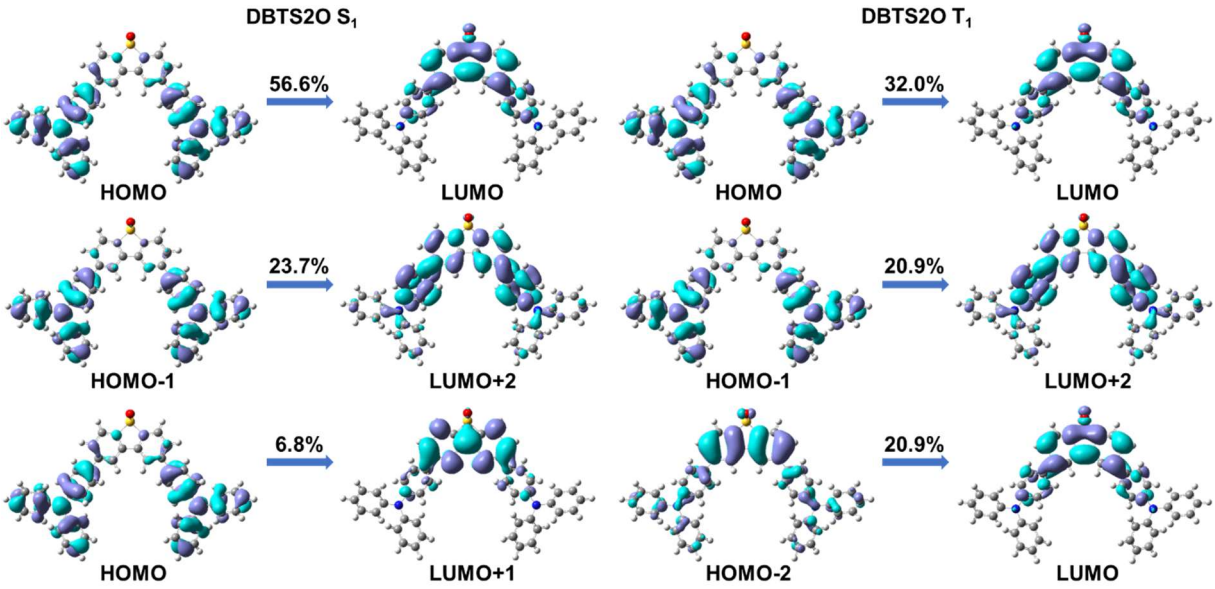

Figure S29. The molecular orbitals of corresponding transition configurations for S_1 and T_1 state of DBTS2O.

Table S2. The S_1 and T_1 state transition configurations of DBTS, DBTSO and DBTS2O revealed by TD-DFT calculations.

		Energy level	Transition configuration
DBTS	S_1	4.04 eV	H → L+1 52.7%, H-1 → L+2 36.2%
	T_1	3.28 eV	H → L+1 40.3%, H-1 → L+2 29.0%, H-3 → L 5.6%
DBTSO	S_1	3.90 eV	H → L 48.8%, H-1 → L+2 27.8%, H → L+1 7.5%, H → L+7 5.7%
	T_1	3.16 eV	H → L 29.0%, H-1 → L+2 21.7%, H-3 → L 18.0%, H → L+7 5.1%
DBTS2O	S_1	3.83 eV	H → L 56.6%, H-1 → L+2 23.7%, H → L+1 6.8%
	T_1	3.11 eV	H → L 32.0%, H-1 → L+2 20.9%, H-2 → L 20.9%

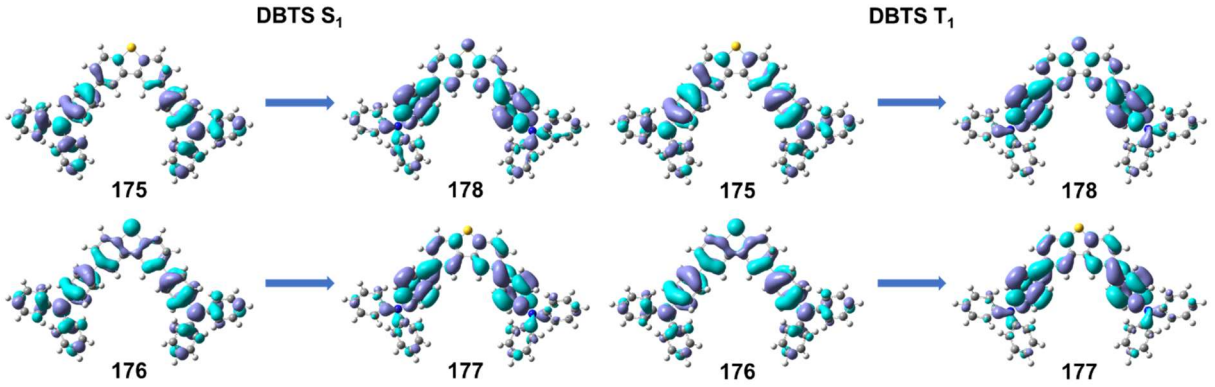

Figure S30. The NTOs for S_1 and T_1 state of DBTS.

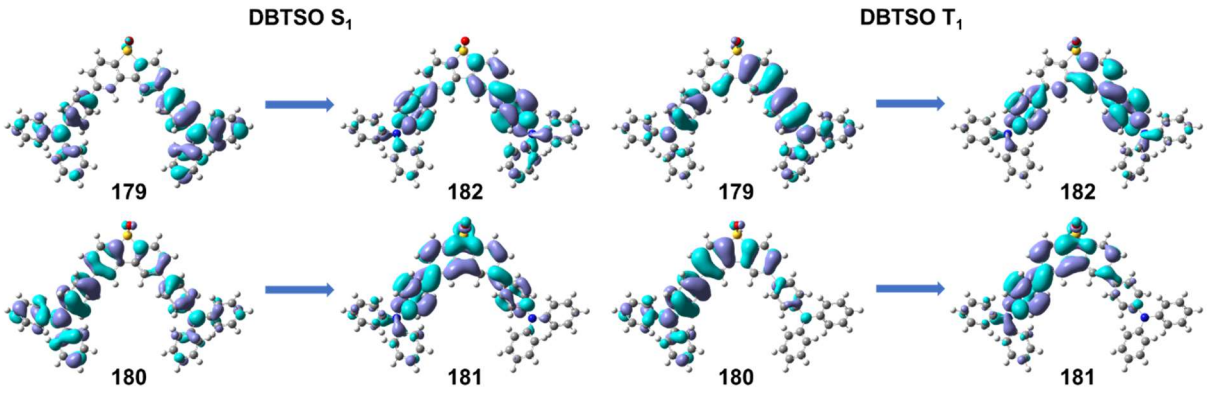

Figure S31. The NTOs for S_1 and T_1 state of DBTSO.

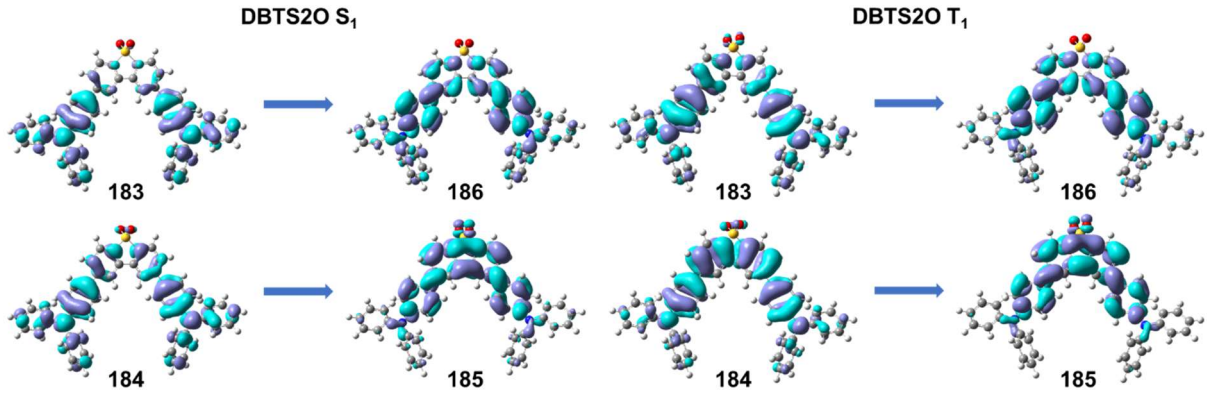

Figure S32. The NTOs for S_1 and T_1 state of DBTS2O.

In DBTS, DBTSO, and DBTS2O, the N atom and S atom exhibit a sp^3 hybridization, and their lone pairs are in the P_z orbitals contributing to the n→π* transition. Meanwhile, the C atom has a sp^2 hybridization, and the P_z orbitals are arranged side by side to form the π bond, contributing to the π→π* transition. Owing to this bonding environment, we further calculated the proportions of (n, π*) or (π, π*) for the S_1 and T_1 state in DBTS, DBTSO, and DBTS2O, using the orbital phase and contribution ratio obtained from NTOs analysis. The results are shown in Table S3-S5.

Table S3. Calculated proportions of (n, π*) or (π, π*) for S_1 and T_1 state of DBTS based on NTOs.

DBTS S_1								DBTS T_1							
175→178 (0.403827)				176→177 (0.551978)				175→178 (0.366319)				176→177 (0.456405)			
Basis	Type	Atom	Composition	Basis	Type	Atom	Composition	Basis	Type	Atom	Composition	Basis	Type	Atom	Composition
31	P_z	2(N)	2.26%	15	P_z	1(S)	0.60%	31	P_z	2(N)	1.53%	15	P_z	1(S)	0.58%
35	P_z	2(N)	5.11%	18	P_z	1(S)	3.34%	35	P_z	2(N)	3.45%	18	P_z	1(S)	3.31%
39	P_z	2(N)	8.62%	21	P_z	1(S)	1.01%	39	P_z	2(N)	6.09%	21	P_z	1(S)	1.09%
532	P_z	44(N)	2.26%	31	P_z	2(N)	1.91%	532	P_z	44(N)	1.52%	31	P_z	2(N)	1.32%
536	P_z	44(N)	5.10%	35	P_z	2(N)	4.32%	536	P_z	44(N)	3.42%	35	P_z	2(N)	2.96%
540	P_z	44(N)	8.61%	39	P_z	2(N)	7.34%	540	P_z	44(N)	6.04%	39	P_z	2(N)	5.25%
				532	P_z	44(N)	1.91%					532	P_z	44(N)	1.33%
				536	P_z	44(N)	4.32%					536	P_z	44(N)	2.99%
				540	P_z	44(N)	7.35%					540	P_z	44(N)	5.30%
^{1}(n, π*) % = 31.96%×0.403827 + 32.10%×0.551978 = 30.62%								^{3}(n, π*) % = 22.05%×0.366319 + 24.13%×0.456405 = 19.09%							
Basis	Type	Atom	Composition	Basis	Type	Atom	Composition	Basis	Type	Atom	Composition	Basis	Type	Atom	Composition
117	P_z	8(C)	0.83%	117	P_z	8(C)	0.72%	117	P_z	8(C)	0.56%	299	P_z	25(C)	1.21%
240	P_z	19(C)	0.76%	240	P_z	19(C)	0.66%	240	P_z	19(C)	0.51%	303	P_z	25(C)	1.00%
299	P_z	25(C)	0.71%	299	P_z	25(C)	0.73%	299	P_z	25(C)	1.32%	355	P_z	30(C)	0.60%
303	P_z	25(C)	0.59%	303	P_z	25(C)	0.62%	303	P_z	25(C)	1.06%	359	P_z	30(C)	1.56%
359	P_z	30(C)	1.06%	359	P_z	30(C)	1.04%	355	P_z	30(C)	0.68%	363	P_z	30(C)	1.83%
363	P_z	30(C)	1.47%	363	P_z	30(C)	1.33%	359	P_z	30(C)	1.75%	419	P_z	35(C)	0.76%
483	P_z	40(C)	0.66%	419	P_z	35(C)	0.52%	363	P_z	30(C)	2.20%	423	P_z	35(C)	0.73%
618	P_z	50(C)	0.83%	519	P_z	42(C)	0.78%	437	P_z	36(C)	0.55%	515	P_z	42(C)	0.78%
741	P_z	61(C)	0.76%	618	P_z	50(C)	0.72%	441	P_z	36(C)	0.72%	519	P_z	42(C)	1.17%
800	P_z	67(C)	0.71%	741	P_z	61(C)	0.66%	479	P_z	40(C)	0.83%	800	P_z	67(C)	1.22%
804	P_z	67(C)	0.59%	800	P_z	67(C)	0.73%	483	P_z	40(C)	1.21%	804	P_z	67(C)	1.00%
860	P_z	72(C)	1.06%	804	P_z	67(C)	0.62%	618	P_z	50(C)	0.56%	856	P_z	72(C)	0.61%
864	P_z	72(C)	1.47%	860	P_z	72(C)	1.04%	741	P_z	61(C)	0.50%	860	P_z	72(C)	1.57%
984	P_z	82(C)	0.66%	864	P_z	72(C)	1.33%	800	P_z	67(C)	1.31%	864	P_z	72(C)	1.85%
				920	P_z	77(C)	0.52%	804	P_z	67(C)	1.05%	920	P_z	77(C)	0.77%
				1020	P_z	84(C)	0.78%	856	P_z	72(C)	0.67%	924	P_z	77(C)	0.74%
								860	P_z	72(C)	1.73%	1016	P_z	84(C)	0.78%
								864	P_z	72(C)	2.19%	1020	P_z	84(C)	1.18%
								938	P_z	78(C)	0.55%				
								942	P_z	78(C)	0.72%				
								980	P_z	82(C)	0.82%				
								984	P_z	82(C)	1.20%				
^{1}(π, π*) % = 12.16%×0.403827 + 12.80%×0.551978 = 11.98%								^{3}(π, π*) % = 22.69%×0.366319 + 19.36%×0.456405 = 17.15%							

Table S4. Calculated proportions of (n, π*) or (π, π*) for S_1 and T_1 state of DBTSO based on NTOs.

DBTSO S_1								DBTSO T_1							
179→182 (0.287602)				180→181 (0.672372)				179→182 (0.241206)				180→181 (0.585448)			
Basis	Type	Atom	Composition	Basis	Type	Atom	Composition	Basis	Type	Atom	Composition	Basis	Type	Atom	Composition
49	P_z	3(N)	3.00%	49	P_z	3(N)	1.00%	49	P_z	3(N)	1.74%	57	P_z	3(N)	0.82%
53	P_z	3(N)	6.76%	53	P_z	3(N)	2.25%	53	P_z	3(N)	3.92%	67	P_z	4(N)	1.99%
57	P_z	3(N)	11.48%	57	P_z	3(N)	3.87%	57	P_z	3(N)	6.94%	71	P_z	4(N)	4.49%
67	P_z	4(N)	1.32%	67	P_z	4(N)	2.79%	67	P_z	4(N)	0.74%	75	P_z	4(N)	7.99%
71	P_z	4(N)	2.98%	71	P_z	4(N)	6.29%	71	P_z	4(N)	1.67%				
75	P_z	4(N)	5.01%	75	P_z	4(N)	10.77%	75	P_z	4(N)	2.96%				
^{1}(n, π*) % = 30.55%×0.287602 + 26.97%×0.672372 = 26.92%								^{3}(n, π*) % = 17.97%×0.241206 + 15.29%×0.585448 = 13.29%							
Basis	Type	Atom	Composition	Basis	Type	Atom	Composition	Basis	Type	Atom	Composition	Basis	Type	Atom	Composition
149	P_z	10(C)	0.55%	395	P_z	32(C)	0.73%	153	P_z	10(C)	0.53%	494	P_z	40(C)	0.56%
153	P_z	10(C)	0.95%	399	P_z	32(C)	0.98%	276	P_z	21(C)	0.59%	512	P_z	41(C)	1.24%
272	P_z	21(C)	0.64%	512	P_z	41(C)	0.63%	331	P_z	27(C)	0.61%	516	P_z	41(C)	1.35%
276	P_z	21(C)	1.07%	516	P_z	41(C)	0.70%	335	P_z	27(C)	1.66%	551	P_z	44(C)	1.03%
335	P_z	27(C)	1.05%	555	P_z	44(C)	0.51%	339	P_z	27(C)	1.36%	555	P_z	44(C)	1.25%
339	P_z	27(C)	0.85%	629	P_z	50(C)	0.73%	353	P_z	28(C)	0.53%	572	P_z	46(C)	0.96%
357	P_z	28(C)	0.53%	633	P_z	50(C)	0.95%	357	P_z	28(C)	0.58%	576	P_z	46(C)	0.79%
391	P_z	32(C)	0.68%	671	P_z	54(C)	1.09%	391	P_z	32(C)	0.94%	607	P_z	49(C)	0.55%
395	P_z	32(C)	1.75%	675	P_z	54(C)	1.33%	395	P_z	32(C)	2.43%	611	P_z	49(C)	1.50%
399	P_z	32(C)	2.33%	685	P_z	55(C)	0.66%	399	P_z	32(C)	3.00%	615	P_z	49(C)	1.33%
438	P_z	35(C)	0.54%	689	P_z	55(C)	1.70%	417	P_z	33(C)	0.51%	625	P_z	50(C)	0.98%
477	P_z	38(C)	0.60%	693	P_z	55(C)	2.35%	434	P_z	35(C)	0.52%	629	P_z	50(C)	2.52%
512	P_z	41(C)	0.53%	749	P_z	60(C)	1.06%	438	P_z	35(C)	0.60%	633	P_z	50(C)	3.01%
516	P_z	41(C)	0.74%	753	P_z	60(C)	0.85%	451	P_z	37(C)	0.50%	667	P_z	54(C)	1.18%
555	P_z	44(C)	0.51%	869	P_z	70(C)	0.62%	455	P_z	37(C)	1.38%	671	P_z	54(C)	3.15%
689	P_z	55(C)	0.58%	873	P_z	70(C)	1.03%	459	P_z	37(C)	1.15%	675	P_z	54(C)	3.75%
693	P_z	55(C)	0.79%	992	P_z	81(C)	0.62%	494	P_z	40(C)	0.95%	685	P_z	55(C)	0.97%
				996	P_z	81(C)	1.03%	498	P_z	40(C)	0.89%	689	P_z	55(C)	2.51%
								508	P_z	41(C)	0.96%	693	P_z	55(C)	3.24%
								512	P_z	41(C)	2.52%	711	P_z	56(C)	0.60%
								516	P_z	41(C)	3.03%	728	P_z	58(C)	0.51%
								547	P_z	44(C)	0.87%	732	P_z	58(C)	0.56%
								551	P_z	44(C)	2.24%	745	P_z	60(C)	0.65%
								555	P_z	44(C)	2.56%	749	P_z	60(C)	1.76%
								590	P_z	47(C)	0.89%	753	P_z	60(C)	1.42%
								594	P_z	47(C)	1.21%	767	P_z	61(C)	0.52%
								689	P_z	55(C)	0.82%	771	P_z	61(C)	0.57%
								693	P_z	55(C)	1.02%	873	P_z	70(C)	0.68%
								749	P_z	60(C)	0.60%	996	P_z	81(C)	0.68%
^{1}(π, π*) % = 14.69%×0.287602 + 17.57%×0.672372 = 16.04%								^{3}(π, π*) % = 35.45%×0.241206 + 39.82%×0.585448 = 31.86%							

Table S5. Calculated proportions of (n, π*) or (π, π*) for S_1 and T_1 state of DBTS2O based on NTOs.

DBTS2O S_1								DBTS2O T_1							
183→186 (0.256578)				184→185 (0.713488)				183→186 (0.266447)				184→185 (0.574434)			
Basis	Type	Atom	Composition	Basis	Type	Atom	Composition	Basis	Type	Atom	Composition	Basis	Type	Atom	Composition
49	P_z	3(N)	2.22%	49	P_z	3(N)	1.89%	49	P_z	3(N)	1.45%	49	P_z	3(N)	1.03%
53	P_z	3(N)	5.01%	53	P_z	3(N)	4.26%	53	P_z	3(N)	3.27%	53	P_z	3(N)	2.33%
57	P_z	3(N)	8.46%	57	P_z	3(N)	7.34%	57	P_z	3(N)	5.78%	57	P_z	3(N)	4.14%
568	P_z	46(N)	2.22%	568	P_z	46(N)	1.89%	568	P_z	46(N)	1.45%	568	P_z	46(N)	1.03%
572	P_z	46(N)	5.01%	572	P_z	46(N)	4.26%	572	P_z	46(N)	3.27%	572	P_z	46(N)	2.33%
576	P_z	46(N)	8.46%	576	P_z	46(N)	7.33%	576	P_z	46(N)	5.78%	576	P_z	46(N)	4.14%
^{1}(n, π*) % = 31.38%×0.256578 + 26.97%×0.713488 = 27.29%								^{3}(n, π*) % = 21.00%×0.266447 + 15.00%×0.574434 = 14.21%							
Basis	Type	Atom	Composition	Basis	Type	Atom	Composition	Basis	Type	Atom	Composition	Basis	Type	Atom	Composition
135	P_z	9(C)	0.70%	135	P_z	9(C)	0.67%	321	P_z	26(C)	0.52%	355	P_z	30(C)	0.55%
258	P_z	20(C)	0.73%	258	P_z	20(C)	0.70%	355	P_z	30(C)	0.74%	359	P_z	30(C)	1.42%
359	P_z	30(C)	1.21%	355	P_z	30(C)	0.53%	359	P_z	30(C)	1.91%	363	P_z	30(C)	1.85%
363	P_z	30(C)	1.60%	359	P_z	30(C)	1.36%	363	P_z	30(C)	2.37%	419	P_z	35(C)	0.93%
419	P_z	35(C)	0.70%	363	P_z	30(C)	1.86%	419	P_z	35(C)	1.27%	423	P_z	35(C)	0.77%
423	P_z	35(C)	0.53%	419	P_z	35(C)	0.79%	423	P_z	35(C)	0.96%	437	P_z	36(C)	1.16%
654	P_z	52(C)	0.70%	423	P_z	35(C)	0.62%	455	P_z	37(C)	0.55%	441	P_z	36(C)	1.04%
777	P_z	63(C)	0.73%	459	P_z	37(C)	0.63%	459	P_z	37(C)	0.63%	451	P_z	37(C)	0.83%
878	P_z	73(C)	1.21%	497	P_z	41(C)	0.87%	497	P_z	41(C)	0.68%	455	P_z	37(C)	2.15%
882	P_z	73(C)	1.60%	501	P_z	41(C)	0.96%	501	P_z	41(C)	0.74%	459	P_z	37(C)	2.48%
938	P_z	78(C)	0.70%	654	P_z	52(C)	0.67%	533	P_z	43(C)	0.59%	493	P_z	41(C)	1.03%
942	P_z	78(C)	0.53%	777	P_z	63(C)	0.70%	537	P_z	43(C)	0.92%	497	P_z	41(C)	2.84%
				874	P_z	73(C)	0.53%	840	P_z	69(C)	0.52%	501	P_z	41(C)	2.99%
				878	P_z	73(C)	1.36%	874	P_z	73(C)	0.74%	515	P_z	42(C)	1.01%
				882	P_z	73(C)	1.86%	878	P_z	73(C)	1.91%	519	P_z	42(C)	0.85%
				938	P_z	78(C)	0.79%	882	P_z	73(C)	2.37%	874	P_z	73(C)	0.55%
				942	P_z	78(C)	0.62%	938	P_z	78(C)	1.27%	878	P_z	73(C)	1.42%
				978	P_z	80(C)	0.63%	942	P_z	78(C)	0.96%	882	P_z	73(C)	1.85%
				1016	P_z	84(C)	0.87%	974	P_z	80(C)	0.55%	938	P_z	78(C)	0.93%
				1020	P_z	84(C)	0.96%	978	P_z	80(C)	0.63%	942	P_z	78(C)	0.77%
								1016	P_z	84(C)	0.68%	956	P_z	79(C)	1.16%
								1020	P_z	84(C)	0.74%	960	P_z	79(C)	1.04%
								1052	P_z	86(C)	0.59%	970	P_z	80(C)	0.83%
								1056	P_z	86(C)	0.92%	974	P_z	80(C)	2.15%
												978	P_z	80(C)	2.48%
												1012	P_z	84(C)	1.03%
												1016	P_z	84(C)	2.84%
												1020	P_z	84(C)	2.99%
												1034	P_z	85(C)	1.01%
												1038	P_z	85(C)	0.85%
^{1}(π, π*) % = 10.94%×0.256578 + 17.98%×0.713488 = 15.64%								^{3}(π, π*) % = 23.76%×0.266447 + 43.80%×0.574434 = 31.49%							

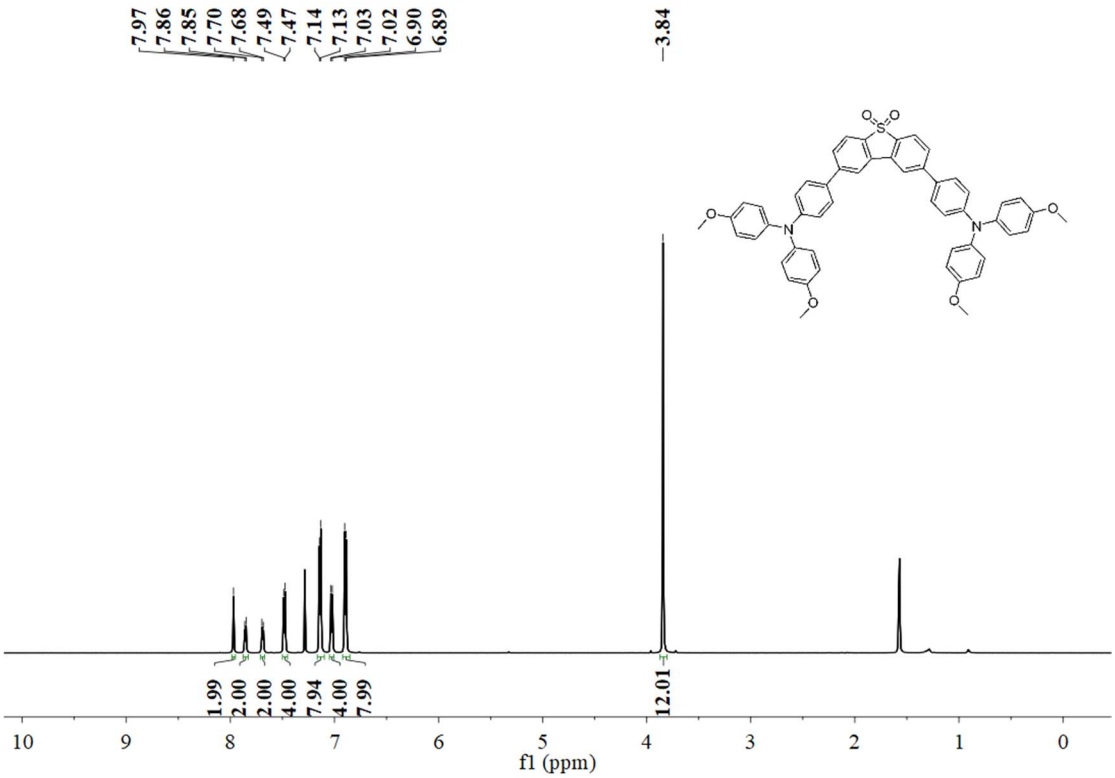

Figure S33. ^{1}H NMR spectrum of compound **4** in $CDCl_3$.

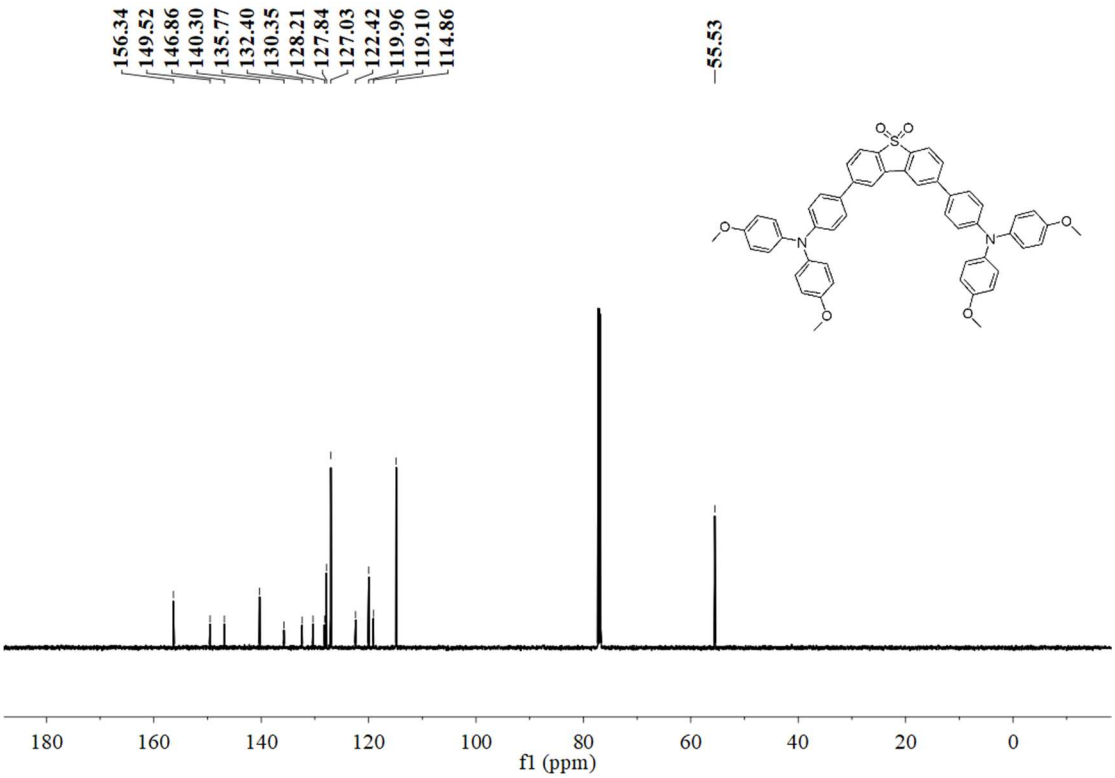

Figure S34. ^{13}C NMR spectrum of compound **4** in $CDCl_3$.

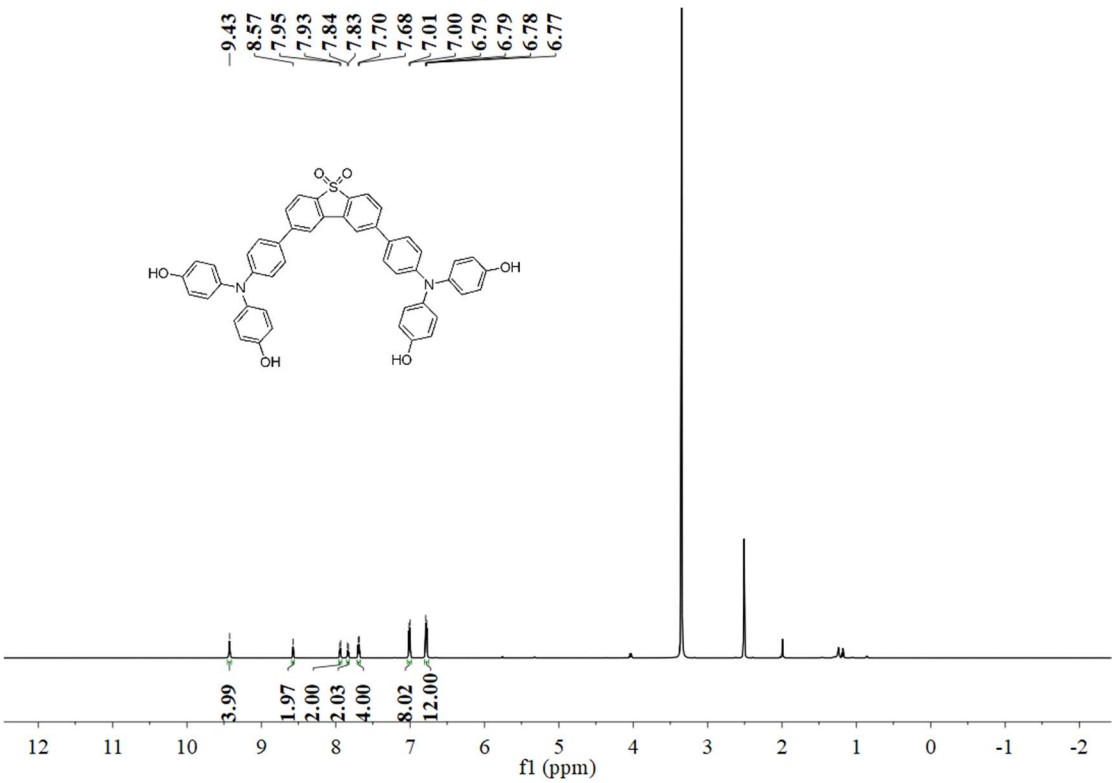

Figure S35. ^{1}H NMR spectrum of compound **5** in DMSO-d_6.

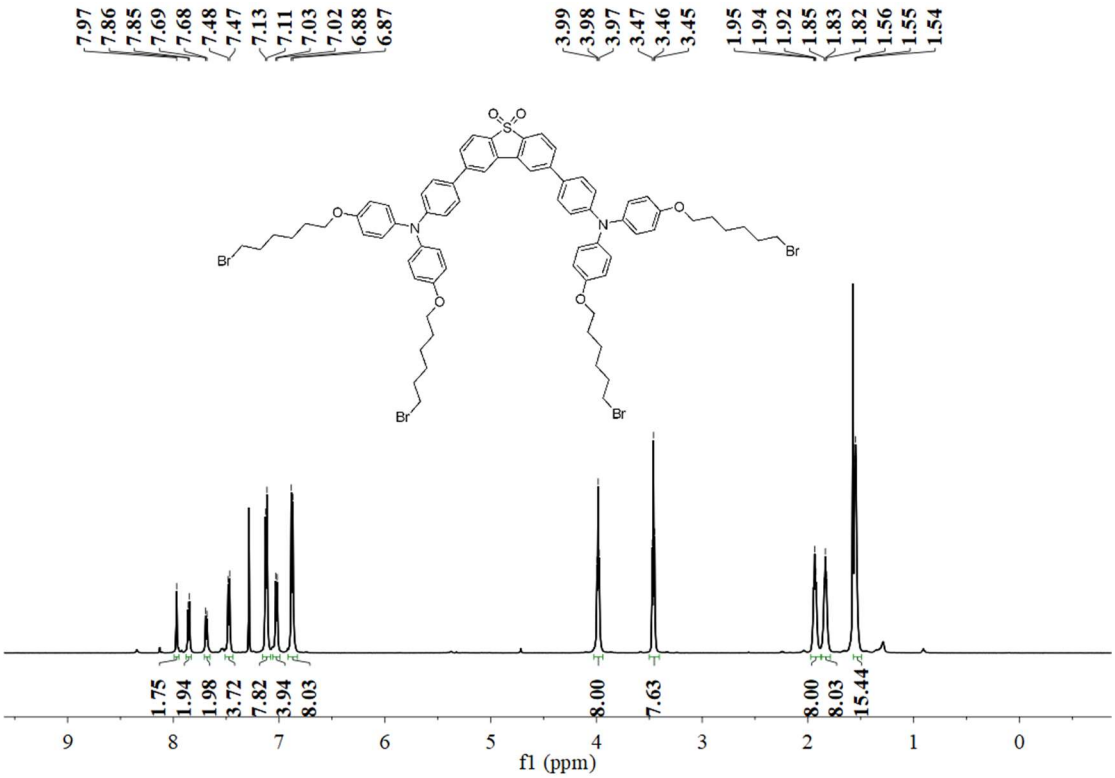

Figure S36. ^{1}H NMR spectrum of compound **6** in $CDCl_3$.

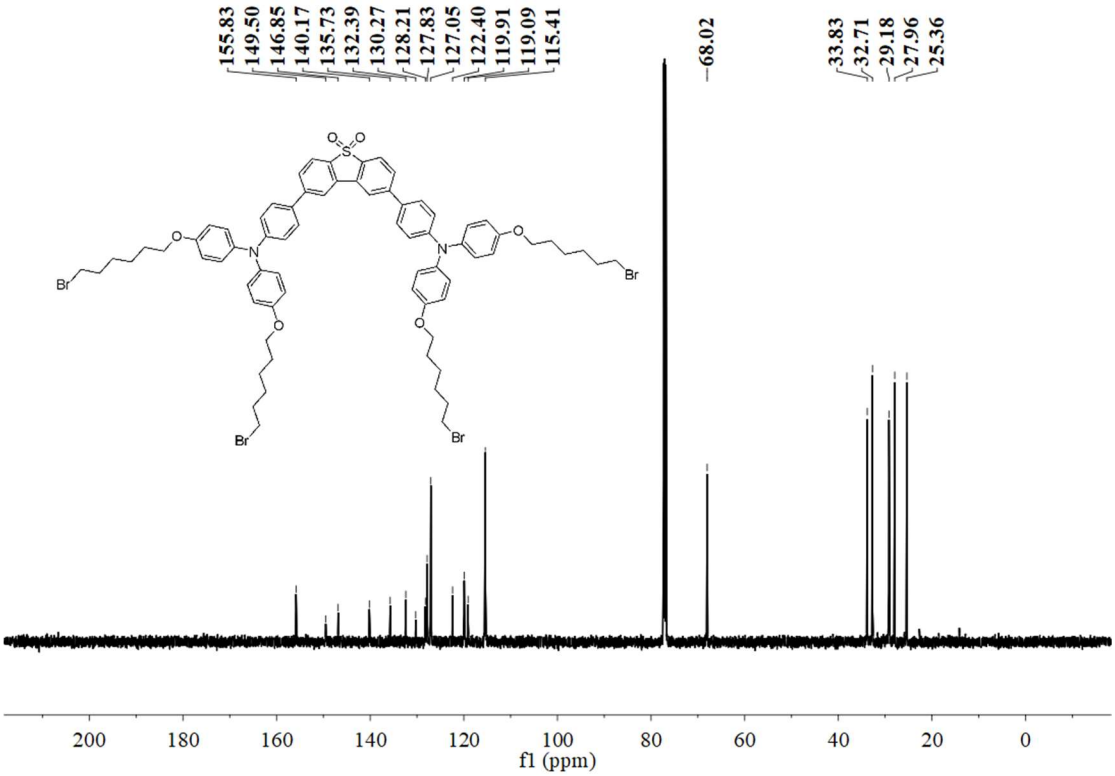

Figure S37. ^{13}C NMR spectrum of compound **6** in $CDCl_3$.

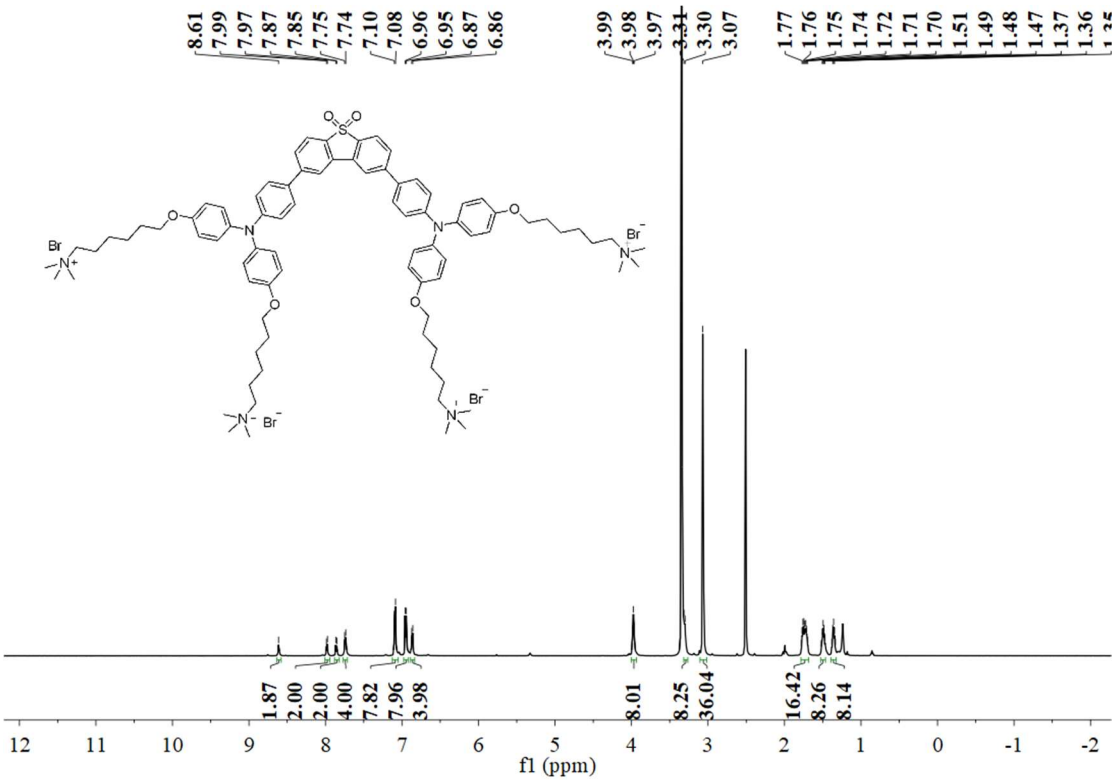

Figure S38. ^{1}H NMR spectrum of 2OA in DMSO-d_6.

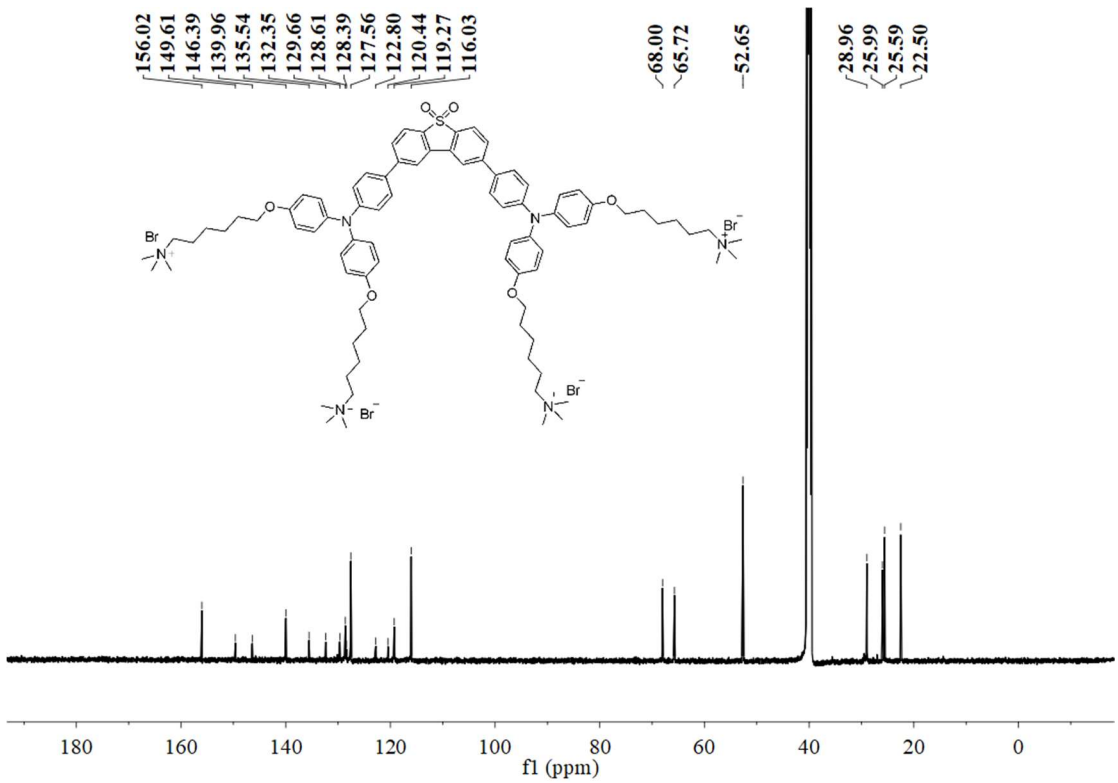

Figure S39. ^{13}C NMR spectrum of 2OA in DMSO-d_6.

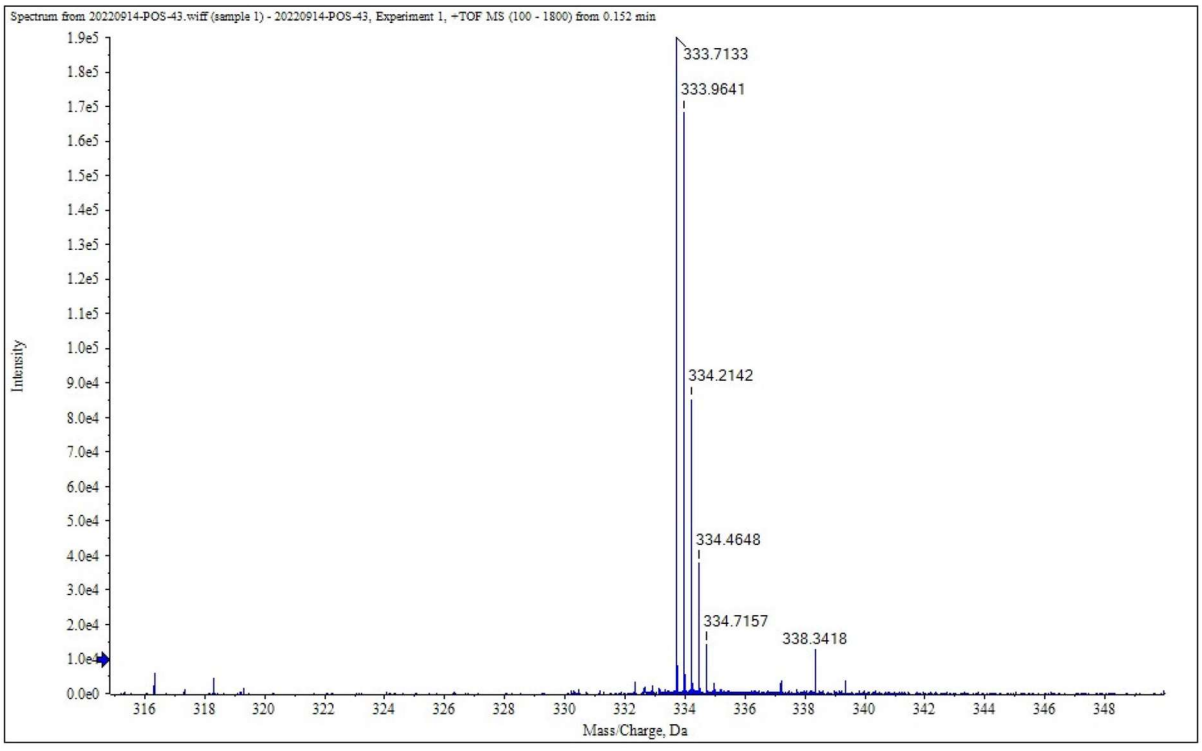

Figure S40. HRMS spectrum of 2OA.

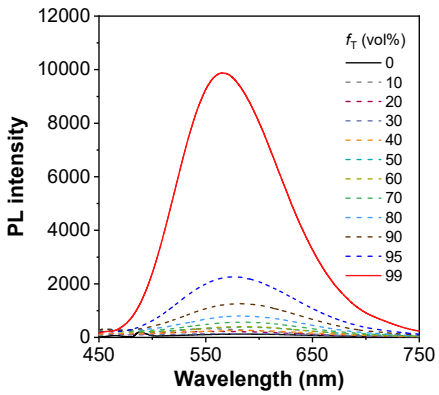

Figure S41. The fluorescence spectra 2OA in water/THF mixtures with different THF fractions (f_T).

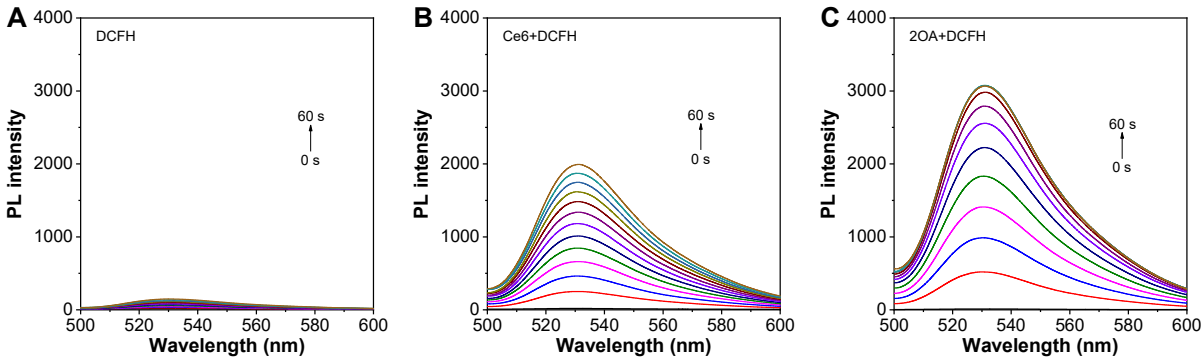

Figure S42. The fluorescence spectra changes of DCFH as the indicator for ROS detection. (A) DCFH alone, (B) Ce6+DCFH and (C) 2OA+DCFH after irradiated to white light (8 mW cm^{-2}) with different time. The concentration of Ce6 and 2OA is 5 μM.

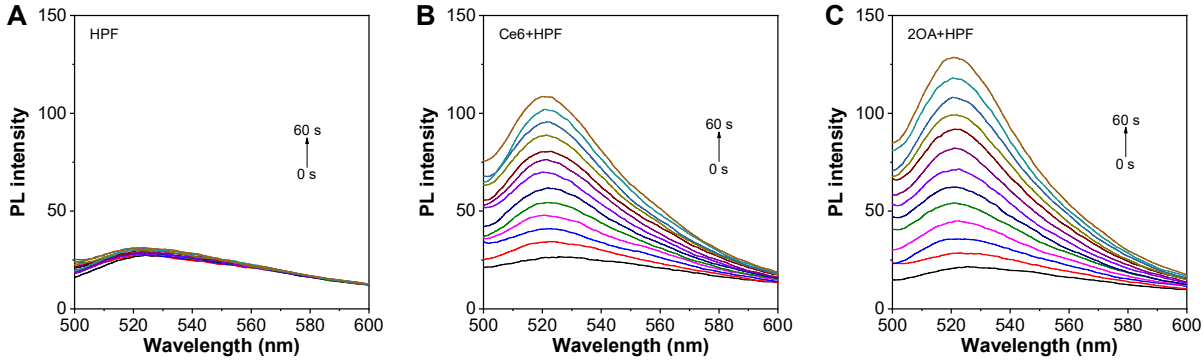

Figure S43. The fluorescence spectra changes of HPF as the indicator for ROS detection. (A) HPF alone, (B) Ce6+HPF and (C) 2OA+HPF after irradiated to white light (8 mW cm^{-2}) with different time. The concentration of Ce6 and 2OA is 5 μM.

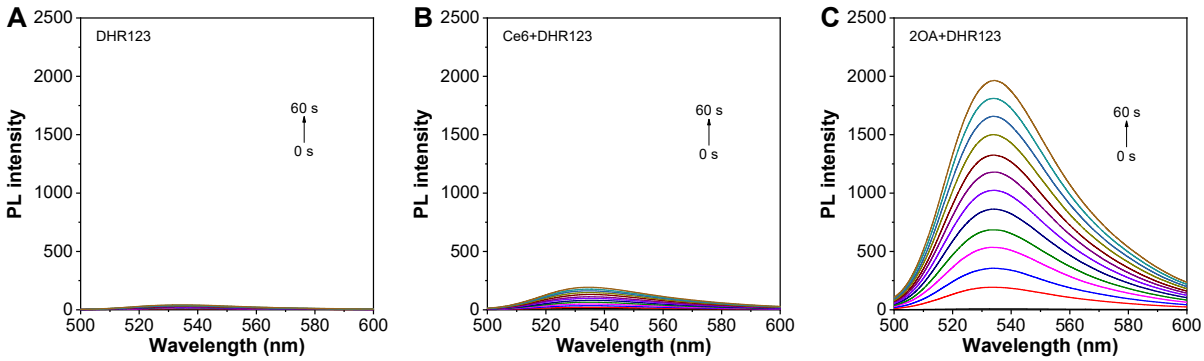

Figure S44. The fluorescence spectra changes of DHR123 as the indicator for ROS detection. (A) DHR123 alone, (B) Ce6+DHR123 and (C) 2OA+DHR123 after irradiated to white light (8 mW cm^{-2}) with different time. The concentration of Ce6 and 2OA is 5 μM.

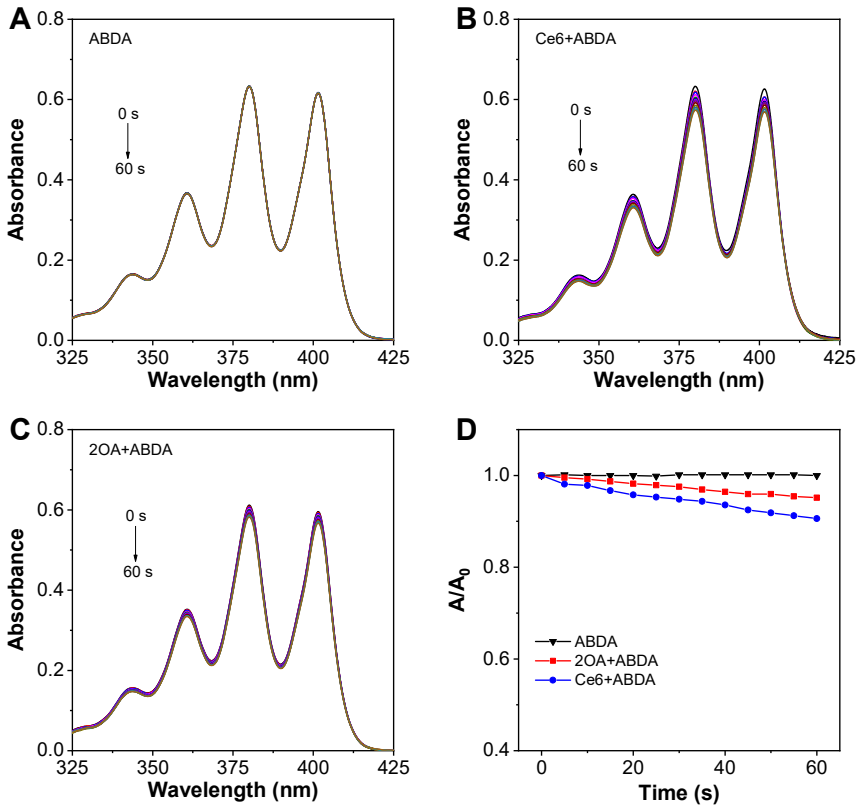

Figure S45. The fluorescence spectra changes of ABDA as the indicator for ROS detection. (A) ABDA alone, (B) Ce6+ABDA and (C) 2OA+ABDA after irradiated to white light irradiation (8 mW cm^{-2}) with different time. (D) Relative changes in absorbance of ABDA without and with Ce6 or 2OA upon white light irradiation for different times. The concentration of Ce6 and 2OA is 5 μM.

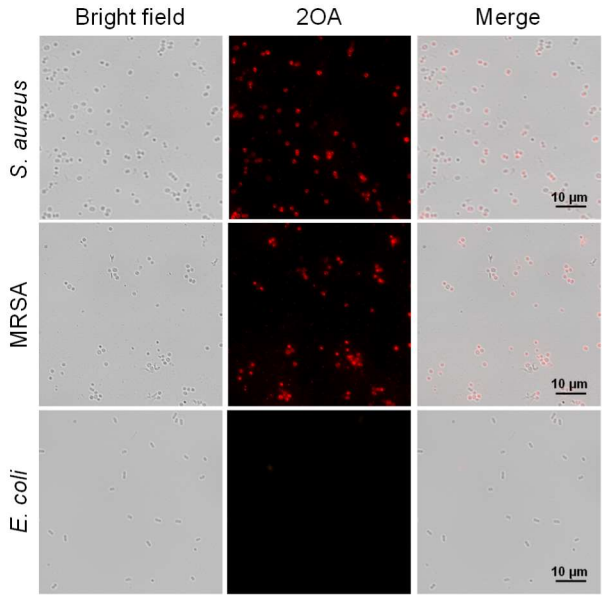

Figure S46. Bright field and fluorescent images of *S. aureus*, MRSA and *E. coli* incubated with 2OA (5 μM).

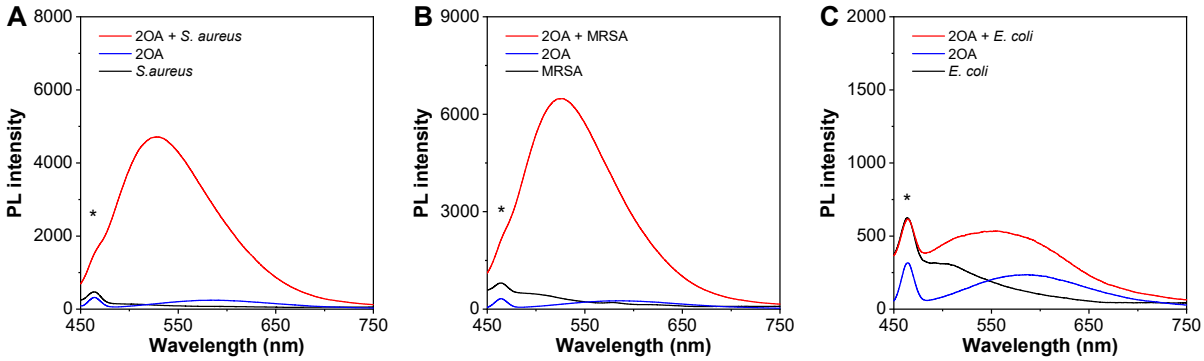

Figure S47. The fluorescence spectra of (A) *S. aureus*, (B) MRSA and (C) *E. coli* solution in PBS (with 1 vol% DMSO) incubated without and with 2OA (5 μM), and 2OA alone (5 μM) in PBS (with 1 vol% DMSO), where the asterisk denotes Raman peak from solvent (and bacteria).

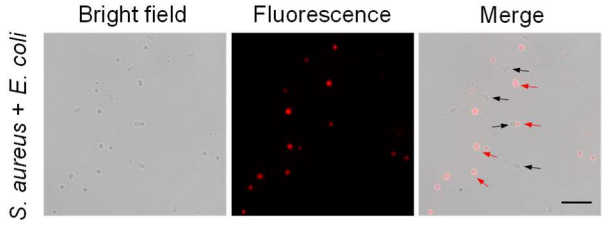

Figure S48. Bright-field and fluorescent images of *S. aureus* + *E. coli* mixture incubated with 2OA (5 μM). The black arrows represent *E. coli* and the red arrows represent *S. aureus*. Scar bar = 10 μm.

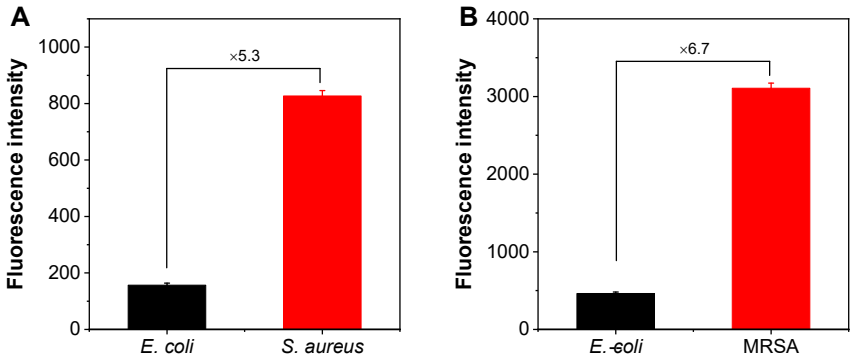

Figure S49. (A) Fluorescence intensity of *E. coli* and *S. aureus* in *S. aureus* + *E. coli* mixture incubated with 2OA. (B) Fluorescence intensity of *E. coli* and MRSA in MRSA + *E. coli* mixture incubated with 2OA.

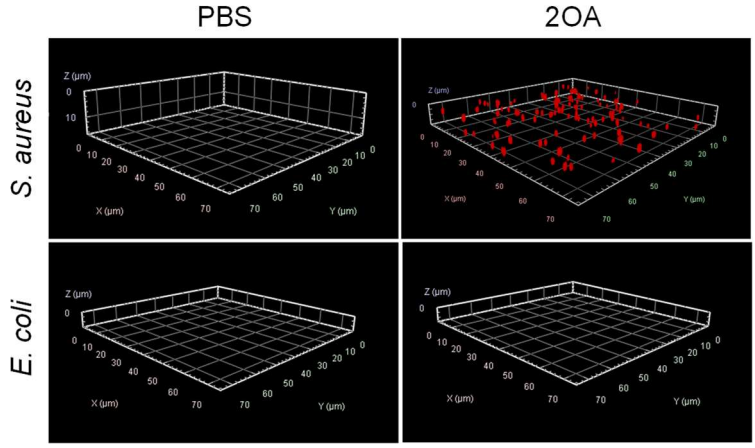

Figure S50. The 3D CLSM images of *S. aureus* and *E. coli* incubated with 2OA (5 μM).

Table S6. Zeta potential of *S. aureus*, MRSA and *E. coli* incubated without and with 2OA (5 μM).

	S. aureus	MRSA	*E. coli*
$\xi_{without\ 2OA}$ (mV)	-28.73±1.50	-28.17±0.69	-23.70±1.80
$\xi_{with\ 2OA}$ (mV)	-19.82±1.37	-19.18±2.81	-24.20±0.57

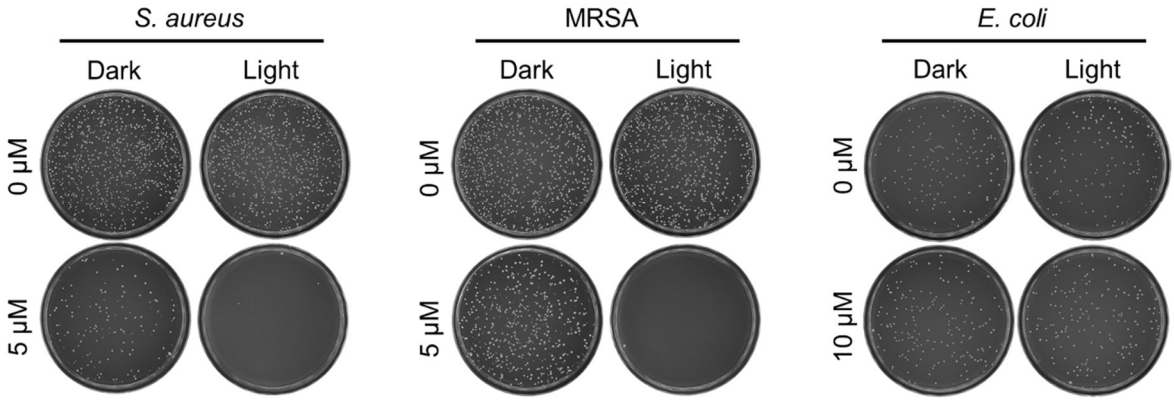

Figure S51. Photographs of *S. aureus*, MRSA and *E. coli* treated with 2OA at different concentrations on the agar plates under dark and light conditions.

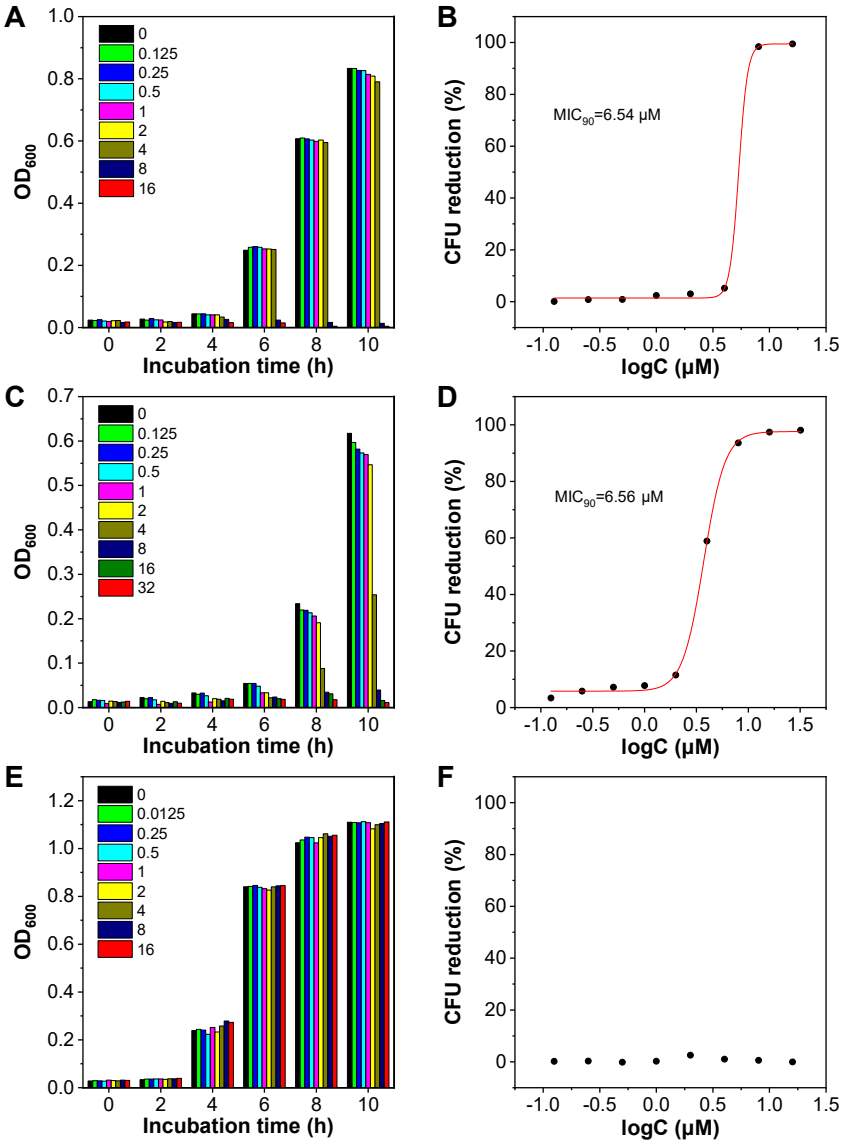

Figure S52. Optical density changes of (A) *S. aureus*, (C) MRSA and (E) *E. coli* incubated with 2OA with different concentrations at different incubation time under light conditions. CFU reduction (%) vs. log(C) plot of light conditions for (B) *S. aureus*, (D) MRSA and (F) *E. coli* at 10 h.

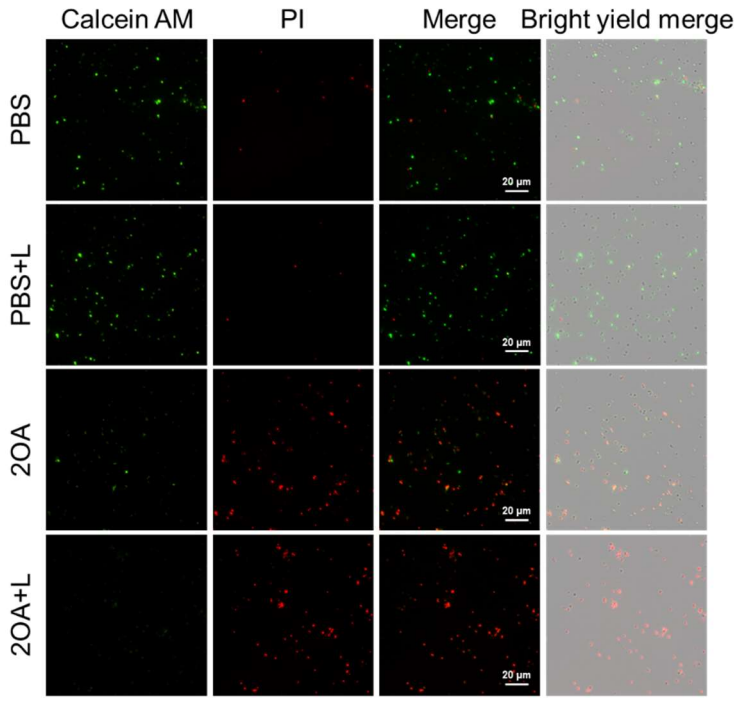

Figure S53. Live/dead bacteria staining images of *S. aureus* treated with PBS or 2OA (5 μM) with/without white light irradiation, where live and dead bacteria were shown in green and red, respectively.

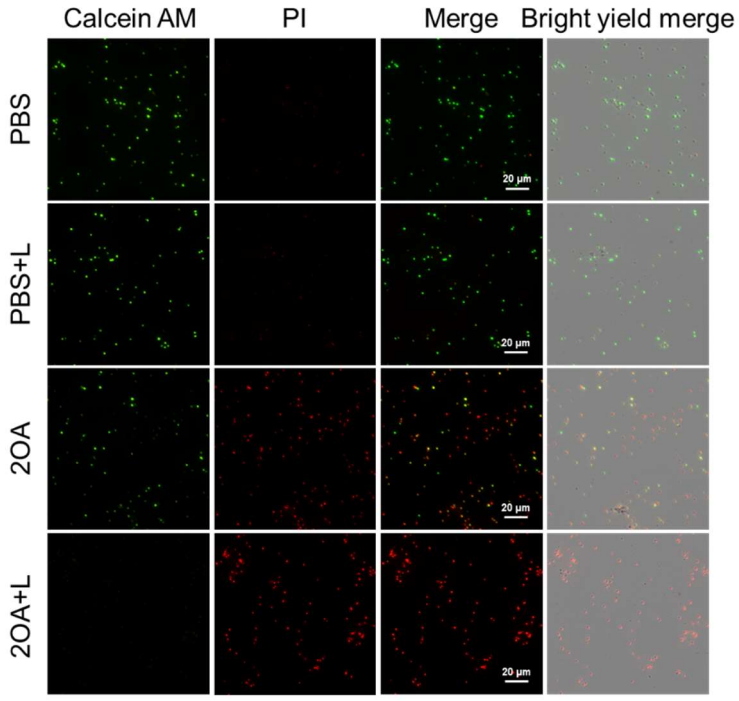

Figure S54. Live/dead bacteria staining images of MRSA treated with PBS or 2OA (5 μM) with/without white light irradiation, where live and dead bacteria were shown in green and red, respectively.

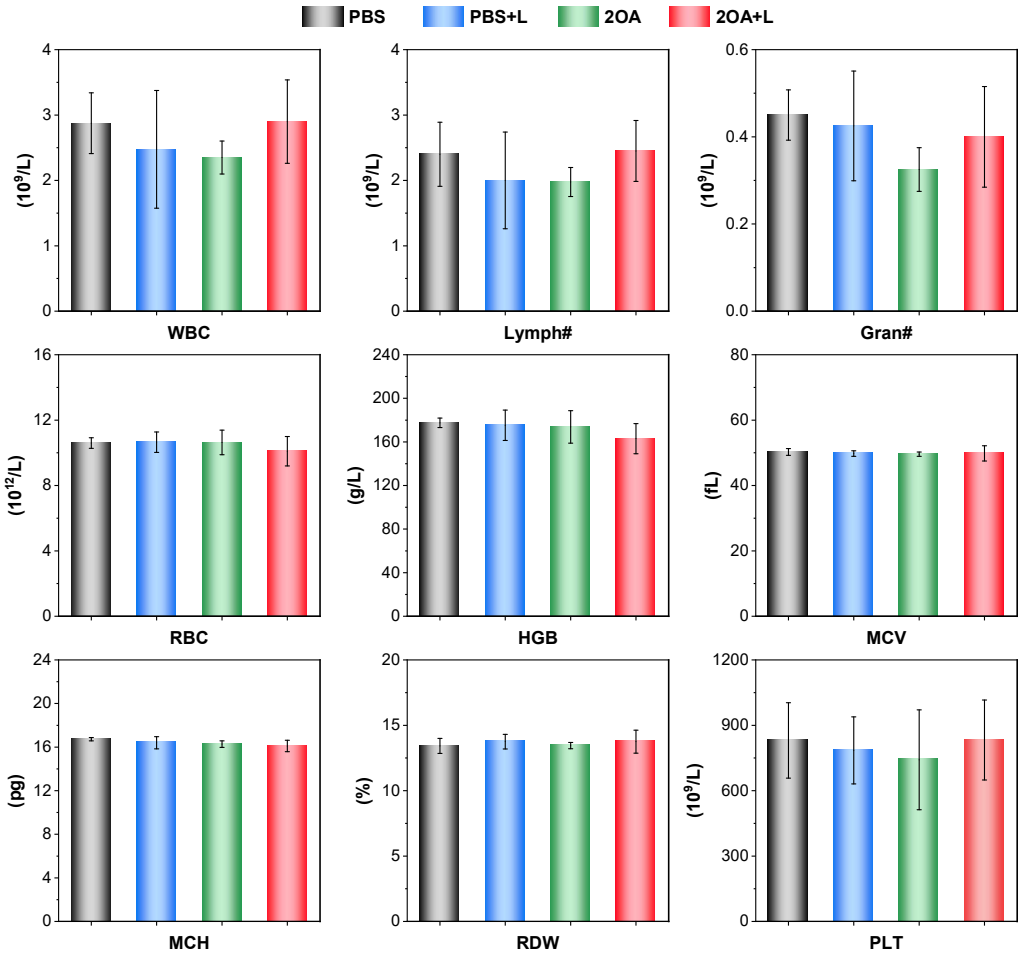

Figure S55. Blood routine assays of MRSA infected mice at day 9 after different treatments.

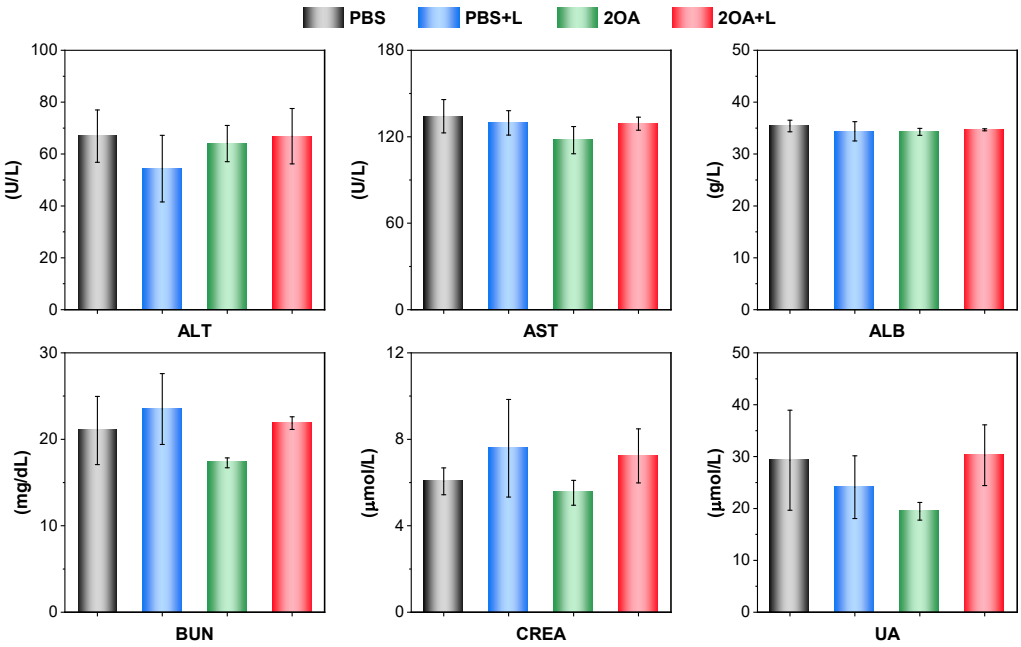

Figure S56. Blood biochemistry test regarding liver and kidney function of MRSA infected mice at day 9 after different treatments.

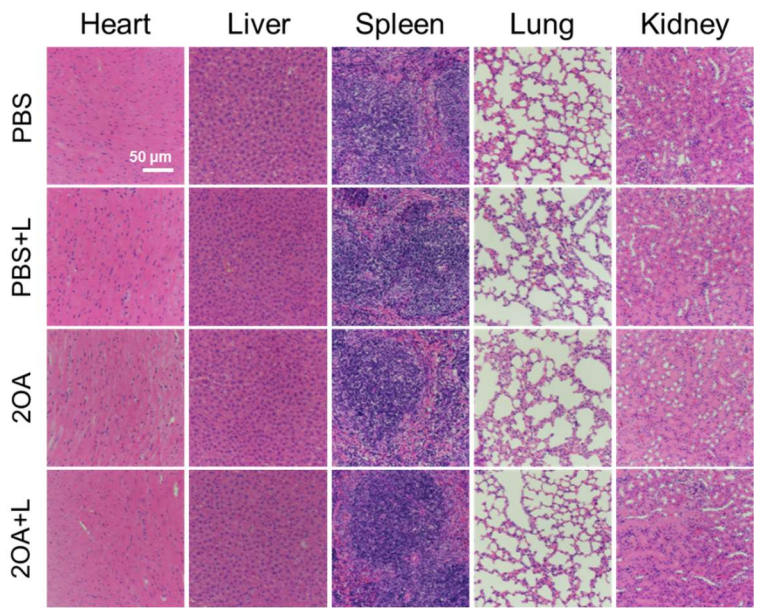

Figure S57. Histological H&E staining of major organs (heart, liver, spleen, lung, kidney) of MRSA infected mice at day 9 after different treatments.

References

[1] M. J. Frisch, G. W. Trucks, H. B. Schlegel, G. E. Scuseria, M. A. Robb, J. R. Cheeseman, G. Scalmani, V. Barone, B. Mennucci, G. A. Petersson, H. Nakatsuji, M. Caricato, X. Li, H. P. Hratchian, A. F. Izmaylov, J. Bloino, G. Zheng, J. L. Sonnenberg, M. Hada, M. Ehara, K. Toyota, R. Fukuda, J. Hasegawa, M. Ishida, T. Nakajima, Y. Honda, O. Kitao, H. Nakai, T. Vreven, J. A. Montgomery Jr., J. E. Peralta, F. Ogliaro, M. J. Bearpark, J. Heyd, E. N. Brothers, K. N. Kudin, V. N. Staroverov, R. Kobayashi, J. Normand, K. Raghavachari, A. P. Rendell, J. C. Burant, S. S. Iyengar, J. Tomasi, M. Cossi, N. Rega, N. J. Millam, M. Klene, J. E. Knox, J. B. Cross, V. Bakken, C. Adamo, J. Jaramillo, R. Gomperts, R. E. Stratmann, O. Yazyev, A. J. Austin, R. Cammi, C. Pomelli, J. W. Ochterski, R. L. Martin, K. Morokuma, V. G. Zakrzewski, G. A. Voth, P. Salvador, J. J. Dannenberg, S. Dapprich, A. D. Daniels, Ö. Farkas; J. B. Foresman, J. V. Ortiz, J. Cioslowski, D. J. Fox, *Gaussian 09, Revision D.01*, Gaussian, Inc.: Wallingford, CT, **2009**.

[2] a) M. A. Spackman, D. Jayatilaka, *CrystEngComm* **2009**, *11*, 19-32; b) M. A. Spackman, J. J. McKinnon, *CrystEngComm* **2002**, *4*, 378-392; c) P. R. Spackman, M. J. Turner, J. J. McKinnon, S. K. Wolff, D. J. Grimwood, D. Jayatilaka, M. A. Spackman, *J. Appl. Cryst.* **2021**, *54*, 1006-1011.

[3] a) C. Lefebvre, G. Rubez, H. Khartabil, J. C. Boisson, J. Contreras-Garcia, E. Henon, *Phys. Chem. Chem. Phys.* **2017**, *19*, 17928-17936; b) T. Lu, Q. Chen, *J. Comput. Chem.* **2022**, *43*, 539-555.

[4] T. Lu, F. Chen, *J. Comput. Chem.* **2012**, *33*, 580-592.

[5] A. D. William Humphrey, and Klaus Schulten *J. Mol. Graphics* **1996**, *14*, 33-38.